In vitro model for Fuchs Endothelial Dystrophy and its effects on corneal endothelial cells

by

Deepak Jain

A thesis

presented to the University of Waterloo

in fulfillment of the

thesis requirement for the degree of

Master of Applied Science

in

Chemical Engineering

Waterloo, Ontario, Canada, 2020

Author’s Declaration

I hereby declare that I am the sole author of this thesis. This is a true copy of the thesis, including any required final revisions, as accepted by my examiners.

I understand that my thesis may be made electronically available to the public.

Abstract

Fuchs endothelial dystrophy (FED), a corneal endothelium disease, is one of the leading causes for corneal transplantation. During disease progression, Descemet membrane's (DM), the corneal endothelial basement membrane, biomechanical properties such as surface topography and stiffness are affected and form guttatas, pillar-like structures, with different geometries and varied stiffness. Corneal endothelial cells become apoptotic and their function is severely hampered. However, the impact of FED guttatas and stiffness on human corneal endothelial cells remains poorly understood. Currently, endothelial cell injection therapy is being developed and the effects of biomechanical cues on cell therapy is largely unknown. Hence, I hypothesized that guttatas and stiffness might affect corneal endothelial cell behavior such as increasing cell apoptosis. The impact of synthetic guttatas (s-guttata) dimensions on corneal endothelial cell behaviour in endothelial cell injection therapy conditions was studied. A significant increase in the cell apoptosis was observed across 20 μm height s-guttatas on different days. S-Guttatas with higher diameter or spacings showed significant late stage apoptosis and the increasing trend was observed in s-guttatas with lower dimensions. Furthermore, these apoptotic cells were localized around the s-guttatas; and the apoptotic population was the highest in the pattern with lower diameter and spacing. Cells surrounding s-guttatas had higher cytoskeletal stress. In addition, preliminary studies on the stiffness of DM was also performed. Cumulatively, FED guttatas have the potential to induce apoptosis.

Acknowledgements

I would like to thank Prof Evelyn Yim, other previous and current lab members, and summer interns for their immense help and contribution throughout the thesis. I would also like to thank Dr. Muhammad Rizwan for his immense help and guidance. In addition, I am also thankful to Prof Jodhbir Mehta and his team especially Dr. Gary Peh and Dr. Gary Yam, for their immense help and contributions throughout the project.

Table of Contents

Author's Declaration ii

Abstract iii

Acknowledgements iv

List of Figures vii

List of Tables vii

List of Abbreviations viii

1. Literature Review 1

1.1 Anatomy and Physiology of cornea 1

1.1.1 Epithelium 1

1.1.2 Corneal epithelial basement membrane 2

1.1.3 Bowman layer 3

1.1.4 Stroma 3

1.1.5 Descemet membrane 4

1.1.6 Corneal endothelial cells 4

1.2 Corneal endothelium pathologies 6

1.2.1 Fuchs endothelial dystrophy 7

1.2.2 FED prevalence 9

1.2.3 FED etiology and molecular mechanisms 10

1.3 FED current treatments and their limitations 13

1.4 Potential future treatments for corneal endothelium dysfunction 17

1.5 Effect of ECM topographical cues and stiffness on the corneal endothelial cells 21

1.6 Cell tension and ROCK signaling in apoptosis 22

1.7 Synthetic guttata model 25

2. Hypothesis and Objectives 28

3. Synthetic *in vitro* model for FED studies and regenerative therapies 29

3.1 Introduction 30

3.2 Materials and Methods 31

3.2.1 Cell Culture 31

3.2.2 Polystyrene and Polydimethylsiloxane (PDMS) synthetic molds fabrication 31

3.2.3 Cell seeding on patterned samples 32

3.2.4 Annexin V staining and quantification 33

3.2.5 TUNEL staining and quantification 33

3.2.6 Cytoskeletal staining 34

3.2.7 Cell location quantification 35

3.2.8 Statistics 35

3.3 Results and Discussion 36

3.3.1 Guttata fabrication through heat embossing 36
3.3.2 Early stage apoptosis in high seeding cell density 37
3.3.3 Early stage apoptosis in low cell density 41
3.3.4 DNA breakage analysis in high cell density on guttatas 44
3.3.5 Apoptotic cells localization on s-guttatas 46
3.3.6 Cytoskeletal stress analysis 48
3.3.7 Apoptosis and their relationship with guttata 51
3.3.8 Cells experienced cytoskeletal stress around guttatas 54
3.3.9 Synthetic guttata model follows native FED DM conditions 54
3.4 Conclusion 55
4. Combinatorial effects of substrate stiffness and topography on corneal endothelial cells 56
4.1 Introduction 57
4.2 Materials and methods 58
4.2.1 Descemet membrane stiffness measurement 58
4.2.2 GelMA+ synthesis and fabrication 59
4.2.3 Cell Culture and cell seeding 60
4.2.4 Cytoskeletal staining 60
4.3 Results and Discussion 60
4.3.1 Peripheral and transition zone Descemet membrane stiffness 60
4.3.2 Cells cytoskeletal analysis on 30% GelMA+ consisting 20µm guttatas 62
4.4 Conclusion 63
5. Conclusions and Future work 65
5.1 Conclusions 65
5.2 Future work and recommendations 66
5.2.1 Synthetic *in vitro* model along with native FED DM for cell apoptosis studies 66
5.2.2 Cell membrane tension studies 67
5.2.3 FED *in vitro* model development using *in vivo* stiffness measurements 69
6. Additional contributions to other projects: 71
7. Publications published from contributions to other projects: 72
8. References: 73

List of Figures

Figure 1: Corneal layers anatomy 2
Figure 2: Examination of the guttata of a patient with Fuchs dystrophy 8
Figure 3: Corneal transplantation types and their transplanted area. 17
Figure 4: Guttata Fabrication on TCPS. 37
Figure 5: B4G12 on s-guttata show higher early stage apoptotic marker expression on Day 1 at higher cell density 39
Figure 6: B4G12 on s-guttata show higher early stage apoptotic marker expression on Day 2 at higher cell density 40
Figure 7: B4G12 cells on s-guttata show higher early stage apoptotic marker expression on Day 1 at lower cell density 42
Figure 8: B4G12 on s-guttata show higher early stage apoptotic marker expression on Day 2 at lower cell density 43
Figure 9: Guttata induces late stage apoptosis 45
Figure 10: Apoptotic cells localize around guttatas. 47
Figure 11: Cells surrounding guttata showed pMLC and phalloidin expression 50
Figure 12: B4G12 cells on s-guttata show higher early stage apoptotic marker expression on Day 7 at lower cell density 53
Figure 13: Transitional DM are stiffer than peripheral DM 61
Figure 14: Pattern and unpattern substrate exhibit normal cytoskeletal staining 63
Figure 15: Annexin V and PI percentage positive B4G12 cells graphs 24h after seeding at a cell density 300k on an unpatterned substrate 69

List of Tables

Table 1: Dimensions of fabricated s-guttatas 32

List of Abbreviations

ABL	Anterior banded layer
AKT	Protein kinase B
CHED	Congenital hereditary endothelial dystrophy
DI	Deionized
DLEK	Deep lamellar endothelial keratoplasty
DM	Descemet membrane
DMEK	Descemet membrane endothelial keratoplasty
DSEK	Descemet stripping endothelial keratoplasty
ECM	Extracellular matrix
EMT	Epithelial to mesenchymal transition
EK	Endothelial keratoplasty
FADD	Fas Associated Via Death Domain
FAS-ERM	Fas cell surface death receptor-ezrin-radixin-moesin
FED	Fuchs endothelial dystrophy
GelMA	Gelatin methacrylate
ICE	Iridocorneal endothelial syndrome
LCST	Lower critical solution temperature
MLC	Myosin light chain
PBL	Posterior non-banded layer
PBS	Phosphate-buffered saline
PDGF	Platelet-derived growth factor
PDMS	Polydimethylsiloxane
PI	Propidium iodide
PNIPAAm	Poly(N-isopropyl acrylamide)
PK	Penetrating keratoplasty
PET	Polyethylene terephthalate
pMLC	Phosphorylated myosin light chain

PPD	Posterior polymorphous dystrophy
PS	Polystyrene
PTEN	Phosphatase and tensin homolog
ROCK	Rho associated protein kinase
s-guttatas	Synthetic guttatas
TGF-β1	Transforming growth factor beta-1
ZO1	Zonula occludens protein 1

1. Literature Review

1.1 Anatomy and Physiology of cornea

The cornea is an avascular and transparent connective tissue with an average horizontal and vertical diameter of 11.5 mm and 10.5 mm in the human eye, respectively.[1] The cornea is a prolate shape structure with an average anterior and posterior curvature of 7.8 mm and 6.8 mm, respectively.[2] Furthermore, the cornea is 0.5 mm thick at the center with a gradual increase in thickness at the periphery.

The cornea provides the first line of defense for the eye by acting as a structural barrier and protects against infections. In addition, its transparent structure serves an important function for the light refraction which contributes to two-thirds of the eye's refractive power. These functions are cumulative effects of its components consisting of six different types of layers i.e. epithelium, Bowman layer the epithelial basement membrane, stroma, Descemet membrane (DM) the endothelial basement membrane, and endothelium by packing in a lamellar arrangement (Fig 1).[1-3]

1.1.1 Epithelium

The epithelium is composed of nonkeratinized and stratified squamous epithelial cells in four to six layers with a 50 µm in thickness. Top two to three cell layers comprised of flat polygonal cells exhibiting apical microvilli and microplicae structures leading to effective spreading of the mucinous layer of the tear film.[4] These cells form tight junctions to prevent toxins, microbes, and tears from entering in to deeper layers of the cornea. Posterior to superficial layer, another two to three cell thick layer consists of cells possessing similar tight junctions. These cells are known as suprabasal or wing cells. In comparison to superficial cells,

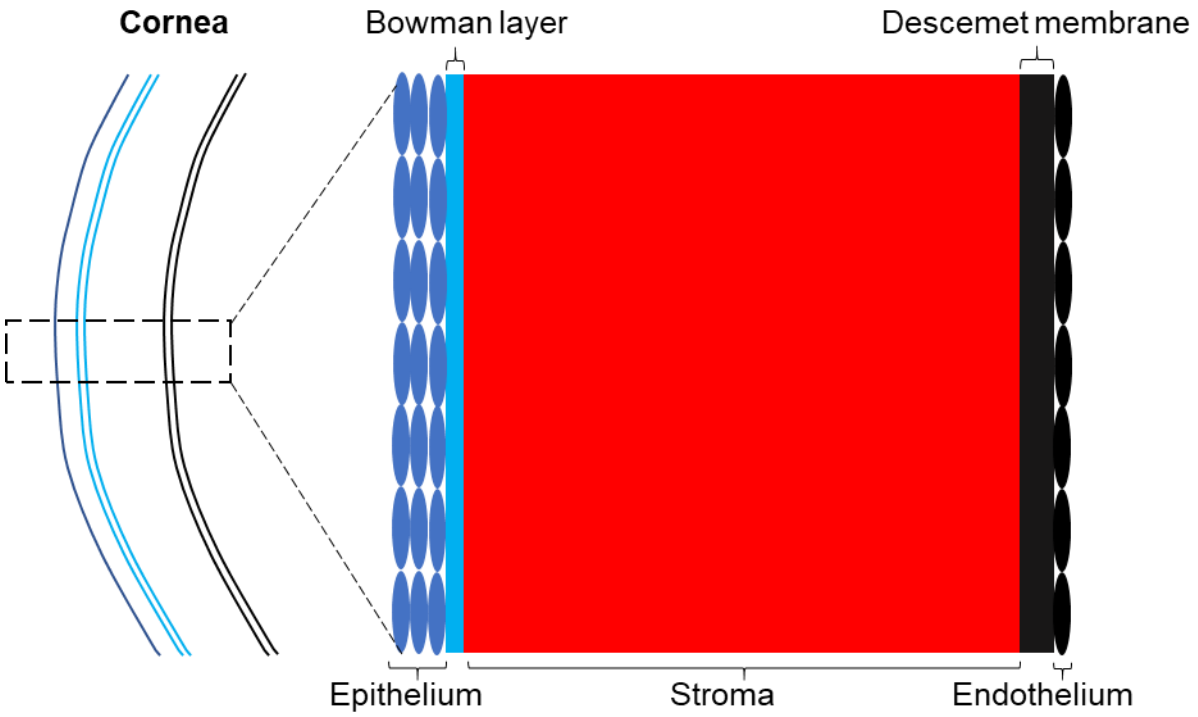

Figure* 1*: Corneal layers anatomy (not to scale)

these cells are relatively less flat in shape. The lowermost epithelial cell layer is known as the basal layer, consists of a single cell layer of columnar epithelial cells 20 µm in thickness.[2] Surrounding basal epithelial cells, the epithelial stem cell population exists in the limbus. These cells differentiate to basal epithelial cells which in turn divides into more mature suprabasal or superficial epithelial cells renewing their population upon cell loss in suprabasal or superficial cell layers.[5] Furthermore, these basal epithelial cells are posteriorly attached to the epithelial basement membrane through a hemidesmosome system keeping the epithelial cells attached to the rest of the cornea.[1, 2]

1.1.2 Corneal epithelial basement membrane

Corneal epithelial basement membrane can be divided in to two different structures: anterior lamina lucida and posterior lamina densa with an 0.05 µm in thickness. Lamina lucida is mainly composed of laminins; while lamina densa consists of heparan sulfate proteoglycans,

collagens, nidogens, and laminins.[6, 7] Basement membranes have been shown to play a role in regulating cell migration, differentiation, and maintenance.[7] Apart from providing structural support, this membrane might also act as a physical barrier to various growth factors such as TGF-β1 and PDGF released in epithelial environment preventing their diffusion to the stroma. As observed by Pal-Ghosh et al., removal of the epithelial basement membrane accelerates the wound healing process.[8]

1.1.3 Bowman layer

This membrane is posterior to the epithelial basement membrane and has an 8-12 μm thickness. It is a non-regenerative acellular condensate of stroma's anterior part. Currently, its role is not completely clear, and it may be superfluous due to the lack of complications in its absence.[2, 9]

1.1.4 Stroma

Another region lying posterior to the Bowman layer is the stroma. It makes up 85-90% of total corneal thickness and contributes to the bulk of the cornea's structural framework. This region is made up of stromal collagen fibers and other components such as inorganic salts, proteoglycans, and glycoproteins. These collagen fibers are made up of parallel bundles of collagen fibrils; heterodimeric complexes of type I and type V collagen. These fibrils are arranged in parallel layers or lamellae; and human stroma consists of 200-250 distinct lamellae.[2] The patterns of collagen lamellae vary with depth where the anterior stroma is composed of narrow and short sheets. Meanwhile, the posterior stroma is mainly composed of long, thick, and wide lamellae.[1, 2] This arrangement provides structural support and also contributes to transparency by preventing light scattering.[10] In addition, keratocytes are the major cell population in the stroma and help in maintaining the extracellular matrix (ECM) integrity by expressing ECM proteins such as

collagen, matrix metalloproteases, and glycosaminoglycans. Furthermore, the stroma also contains macrophages, mature dendritic cells, and immature/precursor-type dendritic cells playing an important role in corneal immunity.[11]

1.1.5 Descemet membrane

The Descemet membrane lies posterior to the stroma and is secreted by corneal endothelial cells. This membrane consists of two different collagen layers: the anterior banded layer (ABL) and the posterior non-banded layer (PNBL). During gestation till birth, the anterior banded layer is deposited reaching a thickness of 3 μm.[12] This ABL is composed of collagen IV and collagen VIII; it is present in between the stroma and PNBL. These collagen structures form multiple layers of stacked hexagonal lattices.[13] These hexagonal lattices form a striated pattern with a periodic gap of 110-120 nm.[14] After birth, collagen VIII expression diminishes, and endothelial cells mainly secrete collagen IV forming a nonstriated and nonlamellar structure, which is known as PNBL. Throughout age, endothelial cells secrete PNBL components resulting in increased DM thickness, which can reach up to 10 μm.[13] The major known function of the DM is to provide structural support to corneal endothelial cells. These cells are attached to the membrane and perceive various biochemical and biomechanical cues.[2, 14]

1.1.6 Corneal endothelial cells

Corneal endothelial cells are derived from neural crest cells and present in a monolayer between the posterior of the DM and the posterior surface of the cornea. These cells are highly active, polygonal, and contain multiple mitochondria organelles. This layer can contain up to 500,000 cells with a density of 6000 cells/mm^2.[14] These cells form a monolayer through shared lateral interdigitations, gap junctions, and incomplete tight junctions. In contrast to the increasing DM thickness, endothelium cell density is inversely proportional to age.[15] Within the first five

years of birth, cell density reduces to 3500 cells/mm^2. This initial reduction in density is majorly due to continuing corneal growth. However, corneal density continues to decline throughout the rest of life at an average rate of 0.06% per year due to continuous endothelial cell loss.[15]

These cells are 5 µm in height and 18-20 µm width comprising the round nucleus 7 µm in diameter.[15] The endothelial cell layer appears in a hexagonal pattern when visualized from the posterior side. The endothelial cells are joined through tight junctions and gap junctions forming a monolayer. In addition, these cells are arrested in the G1 phase and seems to be non-mitotic in nature in the *in vivo* system.[16] Due to non-mitotic nature, cell area and cell size increase upon cell loss to maintain the monolayer structure. The exact cause of this non-mitotic nature is currently unclear; however, it can be due to contact inhibition and cell cycle inhibitors such as p27kip1 as they exhibit proliferative behavior *in vitro*.

Stroma is present in a hydrated state containing 78% water. Along with its higher hydration, its crystalline organization and collagen spacing play a vital role in corneal transparency. However, if fluid accumulates, it will affect its hydration state as well as disrupting its collagen spacing which can degrade the transparency. Hence, the endothelium serves two important functions.[17] First, it helps in maintaining stromal deturgescence by controlling hydration. Second, it also provides nutrients and other metabolites from the aqueous humor to the rest of the cornea. The endothelium serves these functions through a pump-leak mechanism in which the endothelial cell layer acts as a leaky barrier to allow transport of water, ions, and other nutrients from aqueous humor into the stroma. This leaky nature of the membrane is due to incomplete formation of tight junctions such as zonula occludens protein 1 (ZO1). The movement of bulk fluid is passive in nature i.e. it requires no energy, and it is driven through the osmotic process. However, creating this osmosis requires two active ion transport systems such as intracellular carbonic anhydrase

pathway and Na^+/K^+ ATPase ion channels; like bulk fluid movement these systems also drive the flux of ions from aqueous humor to stroma.[1]

1.2 Corneal endothelium pathologies

In the corneal endothelium, cell loss occurs at a relatively constant rate throughout life. Upon cell loss, adjacent cells flatten and spread to cover the defect leading to the desquamation of dead endothelial cells. Due to injury, if the wound size is relatively big, e.g. 2 mm, then distant cells also migrate at a rate of 0.5-1 mm per day.[18] Later, flatten cells begin to recover and try to regain their shape. It causes peripheral endothelial cells to move towards the injured area's center. This pulling process causes changes in neighboring cells' attachment and reformation of junctions. In contrast to quick monolayer restoration in other animal species such as rabbits, complete corneal endothelial cell function restoration can take a long time in humans.[19, 20] However, when the cell density falls below 10-15% of the normal cell population due to injury or pathological conditions, cells are not able to restore the monolayer formation. Failure in corneal endothelial cell function will lead to the hampering of stromal deturgescence maintenance. Due to this, corneal edema occurs and further leads to blindness.

There are a relatively low number of primary corneal endothelial diseases; these include namely posterior polymorphous dystrophy (PPD), congenital hereditary endothelial dystrophy (CHED), iridocorneal endothelial syndrome (ICE), intermediate forms, and Fuchs endothelial dystrophy (FED).[21] PPD is an autosomal dominant and bilateral inherited disease. In this condition, islands of abnormal cells such as epithelial-like cells are present among endothelial cells. The endothelial cell layer further spreads on to the trabecular meshwork and iris. Also, localized or diffused thickening of the DM and the presence of band-like lesions are visualized on the DM. Cumulatively, these can cause calcific and lipid degenerative changes while corneal edema is also

observed in advanced cases.[22] CHED is also a bilateral disease and present in two forms: CHED1 (autosomal dominant) and CHED2 (autosomal recessive). In this disease, endothelial cells are attenuated and appear fibrotic, and the DM is also thickened.[23] CHED1 symptoms are similar to PPD, and it has been suggested that it is a type of PPD with an early onset. Meanwhile, in CHED2, corneal opacification and edema formation is observed at the time of birth or shortly thereafter.

ICE, a unilateral disease, comprised of endothelium in a "cobblestone" shape. Patches of endothelial cells possess epithelial-like features such as cytokeratin markers and microvilli. These abnormal cells are smaller, commonly found in patches, and a relatively higher number. These changes can cause corneal edema and secondary glaucoma.[24] In contrast, "intermediate forms" is the category where an abnormality doesn't correspond to any specific endothelium pathology or a combination of multiple pathologies such as the prevalence of both PPD and partial ICE syndrome.

1.2.1 Fuchs endothelial dystrophy

FED is the most common corneal endothelial disease and it was first defined by Professor Ernst Fuchs as "Dystrophia epithelialis corneae". It's mostly an age-related progressive disorder primarily affecting corneal endothelium and DM.[25] In this disease, abnormal ECM material deposits on the posterior surface of the DM to form wart-like structures known as guttae or guttata (Fig 2).[26-28] Guttatas can be several microns in size and they start to appear in the cornea's centre in the FED's early stage. They are pillar-like or convex micro dome-like structures with varying spacing, height, and diameter. Over the progression of the disease, guttatas further extend to the periphery of the DM and coalesce with each other to form large guttatas. In addition, the thickness of the DM also changes due to the deposition of abnormal posterior banded collagen layers.[29]

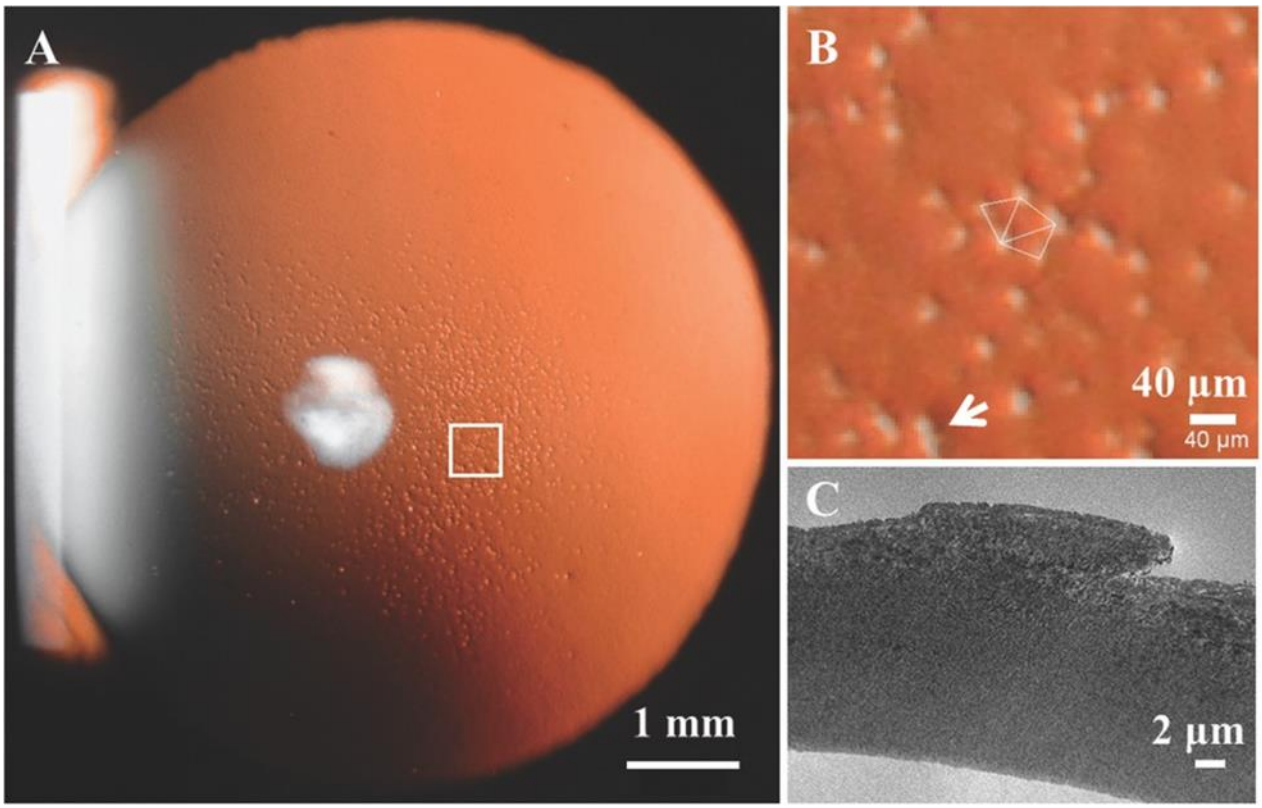

Figure 2: Examination of the guttata of a patient with Fuchs dystrophy. (Copyrights obtained from Rizwan et al, 2016 [28])

Furthermore, in this disease, the progressive loss of endothelial cells also results in higher than normal cell loss during to aging. This leads to the thinning of remaining endothelial cells, decrease in ATPase pump activity, and formation of gaps in monolayer, which cumulatively affect corneal endothelial function. This disease has been categorized into three stages based on signs and symptoms.[30] In the first stage, patients are asymptomatic and isolated guttatas are present at the center of the DM, which is similar to the presence of pigmentation at the peripheral side of the normal cornea. With the progression of the disease, guttatas and the normal endothelial monolayer hexagonal structure deforms in the central part of the cornea. Guttatas spread from the central to the peripheral part of the DM and the area losing hexagonal shape is also increased.[31] In the second stage, due to hindrance in the functionality of endothelial cells, edema starts to form. Initially,

edema may seem to appear in front of the DM. As the disease progresses, the stroma attains a ground-glass appearance and stromal and epithelial edema develops.[30] Visual acuity is compromised leading to the development of symptoms such as glare, blurred vision, and colored halos around light.[30] In addition, patients may experience severe pain due to the rupture of sinus bullae producing corneal erosions. Meanwhile, in the last stage, subepithelial connective tissue forms and epithelial edema is reduced. Visual acuity is severely compromised and peripheral corneal vascularization might develop.

1.2.2 FED prevalence

FED is prevalent in all parts of the world. In a recent survey, 184,756 corneal transplants were done worldwide in 2012.[32] Out of these transplants, 39% are done on patients suffering from FED. In addition, in a smaller subset at the University of Toronto, it was observed that 40% of the corneal transplants were due to FED and the leading cause of corneal transplant.[33] Similarly, the most corneal transplants (18.9%) done in British Columbia were on patients affected by FED. A 12-year study done in France shows that FED is the main reason for 15.1% of corneal transplants.[34] However, the prevalence of this disease is based on ethnicity and age. A study done on 1,016 patients showed that 31% of patients under the age of 40 had guttatas while more than 99% of these patients had a very early form of guttatas. Meanwhile, more than 70% of patients above the age of 40 had guttatas and 4% of these patients had mild to severe form of guttatas.[35] Similarly, a study was conducted on 64 families (228 participants) with a record of FED patients in the family.[36] It was observed that 38% of the patients above the age of 40 had FED symptoms. Furthermore, a study done on the inhabitants of Reykjavik (Iceland) estimated presence of guttatas in 7% of Caucasian male participants and 11% of Caucasian female participants.[37] In the US, a study done on the 148 inhabitants of Tangier Island found that 22% of these participants above the

age of 30 had guttatas present in their eye.[38] In contrast, Asians are less affected by FED. In Japan, guttatas were observed in 2.4% of male and 4.8% female participants. Meanwhile, in Singaporean Chinese, the ratio was slightly higher i.e. 4.4% males and 8.5% females.[27] Cumulatively, it shows FED has a varied prevalence across different sections of society.

1.2.3 FED etiology and molecular mechanisms

FED is well characterized for its diagnosis, symptoms, and treatments. However, the etiology of this disease is not well understood. Many major factors can contribute to the disease such as genetics, abnormal extracellular matrix formation, and intracellular molecular dysfunction.

Genetics: FED has been reported as a heritable disease with a heritability estimate of 37-39% within a family.[39] Its inheritance pattern is established as autosomal dominant. FED genetic nature is quite heterogenous as mutations in different genes have been reported. *Col8A2* mutations are reported to be identified in the early onset FED (a rare form of FED) and late-onset FED.[40, 41] Collagen VIII plays a dominant role in the formation of the DM during developmental stages. Abnormality in the expression of collagen VIII in developmental or late stages in life might affect cell attachment or their function.[42] The most common form of mutations found in the FED group is related to the *TCF4* gene sequence. One type of mutation in *TCF4* is a single nucleotide polymorphism and the other is the presence of multiple CTG repeat sequences in intron 3. These repeats were found in 62-79% of FED patients in Europe and USA, 25% of FED patients in Singapore, and 17-34% of FED patients in India.[43] These mutations don't have much effect on protein functionality; however, they led to the accumulation of RNA transcripts containing CUG repeats in the endothelial cell nucleus which further causes sequestering and functional depletion of RNA splicing factors. This leads to global mis-splicing events throughout the endothelial cell. In addition to these genes, functional mutations in genes such as *SLC4A11* (a co-transporter gene),

ZEB1 (a transcription factor), *Pitx2* (a transcription factor), *LOXHD1* (targeting proteins to the plasma membrane), AGBL1 (codes deglutamylase enzyme) and many more, are also found. These genes play crucial roles in endothelial cell maintenance, function, and appropriate gene regulation.

Intracellular molecular dysfunction: Endothelial cells constantly have active ion channels functioning which creates a higher metabolic need and thus are more prone to metabolic-related stress-induced damages. In addition, these cells are directly exposed to UV irradiation from the sun making them more prone to damages. Another prominent feature that can contribute to the accumulation of stress-induced damage in the non-mitotic nature of cells. It can lead to the accumulation of oxidative related damages in DNA due to the non-replication of the genome. Various studies have noticed irregularities in mitochondrial function as well as the balance of the oxidant-antioxidant mechanism during FED. It has been shown that there is a significant decrease in the expression of antioxidant related genes such as SOD2, Prx2/3/5, TXNDR1 and MT3 and a significant increase in DNA damage and cell apoptosis in FED endothelium.[44, 45] In addition, FED endothelial cells also showed a higher apoptotic cell rate in comparison to normal corneal endothelial cells when both were treated with oxidant species inducers such as tBHP.[46] Furthermore, the expression of oxidants such as hydrogen peroxide as well as oxidative DNA damage was significantly higher in treated FED endothelial cells. These oxidative insults are related to mitochondrial related damages as it is shown that oxidative DNA damages also affect mitochondrial DNA, in addition to nuclear DNA.[44] Mitochondria plays an important role in maintaining the metabolic requirements of a cell. The corneal endothelium consists of numerous mitochondrial organelles in comparison to normal cells due to its energy requirements. However, during FED, there is a significant downregulation of mitochondrial genes related to electron transport and oxidative phosphorylation pathways.[26, 45] When FED corneal endothelial cells are

exposed to oxidative inducing reagents, mitochondrial density, mitochondrial membrane potential, and ATP production decreases.[44, 47] This exposure can further lead to mitochondrial fragmentation.

In contrast to the decrease in expression of crucial antioxidant and mitochondrial-pathway related genes in FED, it has also been observed that the number of misfolded proteins also increased including higher expression of multiple proteins.[48, 49] The authors also observed the presence of rough endoplasmic reticulum in all FED samples as compared to one-third of control samples suggesting the presence of increased protein folding machinery in FED cells. Furthermore, they also observed the expression of markers of unfolded protein response mechanisms such as GRP78, phospho-eIF2a, and CHOP.

In addition to protein machinery, microRNA also plays a vital role in normal cell function and if dysregulated then they can be potential partners for causing numerous diseases.[50] Along these lines, it has been observed that there is a global downregulation of micro-RNAs in FED cells as 87 miRNAs significantly downregulated.[51, 52] This list included ECM protein expression regulating micro-RNAs such as miR-29 family which correlates to the higher expression of ECM related genes in FED cells. Meanwhile, there is no significant increase in the expression of other miRNAs.

Along with cell apoptosis, different studies have also observed the epithelial to mesenchymal transition (EMT) of endothelium cells during FED.[43, 53, 54] Using FED cell lines, Okumura et al. have shown an upregulation of EMT inducing genes such as ZEB1 and SNA1 which increases the expression of ECM proteins through the TGF-β pathway.[53] Similarly, Katikireddy et al. observed that inducing oxidative stress in corneal endothelial cells leads to cell death and EMT induction as well as expression of EMT inducing genes.[54]

Abnormal ECM deposition: Increased expression of ECM proteins such as collagen IV by FED cells lead to deposition of these proteins on the DM, which is reflected in increased membrane thickness as well as guttata formation. Clinically, the density of the guttatas is correlated with the severity of the FED disease. These guttatas are graded from 0 to 5; where 0 means no presence of guttatas and 5 means the presence of confluent guttatas in widespread carpet form.[55, 56] It is shown that the presence of a large number of guttatas in patients is directly proportional to the loss of corneal endothelial cells. Guttatas displace the endothelial cell bodies to their periphery in a rosette type structure as well as some cells adhere to the apex of the guttata.[57, 58] Cells present on the top of guttata are extremely thin and stretched containing little or no cytoplasm. In addition, these cells contain rough endoplasmic reticulum and mitochondria in the nuclear region; and their pump function might be not intact. A cell nucleus surrounding guttata tend to become more rounded in comparison to their normal oval shape and their cytoplasm acquire a degenerative and swollen appearance.[58]

Clusterin (a marker for cell stress) and TGF-β1 (regulating cell growth and EMT) are distinctively localized intracellularly in the cells surrounding guttatas.[59] Furthermore, it has also been observed that endothelial cells seeded on the FED DM consisting of varying guttata diameter can induce cell apoptosis as well as induce expression of EMT related genes.[60] However, it has been noted the DM extracted from FED patients also consists of molecules associated with inflammation, ageing, and oxidative stress such as glycation end products.[26]

1.3 FED current treatments and their limitations

Although, FED disease symptoms and characterization are well known. The treatment options for this disease are very limited. For mild to severe FED conditions, the symptoms are managed by using topical nonsteroidal anti-inflammatory drugs or dehydrating agents.[61] However, these

treatments do not cure FED and there are no clinically available pharmaceutical treatments to cure FED. The only option available for FED treatment is corneal transplantation. Initially, penetrating keratoplasty (PK) was commonly used on FED patients where the whole cornea is replaced with the cornea of a donor (Fig 3). This method is useful as it can address the defects present in the overall cornea. However, there are various post-surgical complications that have been reported after this treatment. There are several reports of high irregular astigmatism, immunological rejection, microbial keratitis, and glaucoma in patients after PK.[62, 63] In addition, the long-term survival rate of the graft is not certain as it can vary a lot from as low as 20% to the highest 98.8% within 10 years after operation.[64] The major cause of PK graft failure is the endothelial decomposition. It has been observed that endothelial cell number continuously decreases with time after PK and this loss follows a biexponential decay pattern.[65]

The advancement of new technologies such as microkeratome and surgical methods led to the development of endothelial keratoplasty (EK). This surgical technique selectively replaces the corneal endothelium which was not possible in PK. In contrast to PK, this technique utilizes a smaller incision, eliminates long-standing sutures, preserves corneal sensation, and decreases the time for visual rehabilitation.[66] Due to these major advantages over PK, EK has currently become a gold standard for FED treatment.[61] The first type of EK developed was deep lamellar endothelial keratoplasty (DLEK). This surgical technique involves an incision of 5-9 mm in the patient's cornea and a lamellar dissection is performed to excise endothelium, DM, and posterior stroma. Similarly, the required posterior part of the cornea is dissected with a trephine to acquire the desired diameter. After dissection, this donor part is transferred to the recipient patient.[67]

DLEK is much preferred over PK. However, excision of the posterior cornea and manual lamellar dissection are quite challenging. Hence, within a few years, a new EK technique was

developed, i.e. Descemet stripping endothelial keratoplasty (DSEK).[68] In this surgical technique, a 3-5 mm incision is made in the recipient's limbal or corneal/scleral section to remove DM and endothelium. This technique reduces tissue excision while keeping intact most of the stromal region. Meanwhile, donor tissue is prepared by manual dissection, microkeratome or a femtosecond laser for desired thickness and diameter. This donor tissue is transferred to the recipients and pressed against the stroma to promote its attachment. Similar to DLEK, this method has various advantages over PK.[69] However, surgical risks such as graft dislocation, endothelial cell loss, graft survival, and visual acuity are also similar to PK.

For FED treatment, these techniques involve excessive tissue. PK involves the whole cornea while DLEK and DSEK involve the posterior cornea. To further reduce the excision of excessive healthy tissue, Descemet membrane endothelial keratoplasty (DMEK) is developed.[70, 71] It involves the transplantation of DM while keeping the stroma intact. In this technique, DM attached to the endothelial cell layer is peeled off from stroma using forceps or pneumatic dissection technique. This healthy donor graft is transplanted in recipients after removing diseased corneal endothelium and DM. Once inside the eye, the graft is oriented and positioned using salt solutions or air bubbles. DMEK shows better outcomes as compared to the above-mentioned techniques. It is superior to DSEK in decrease loss of endothelial cells, inducing less refractive index changes, higher visual acuity, faster visual recovery time, and rejection rates.[72] However, there are many challenges and limitations faced by surgeons for this technique such as rigorous training required for graft preparation, the fragility of donor tissue, unrolling of the graft in the anterior chamber, and postoperative detachment issues.[66]

These transplantation treatments are available everywhere in the world. However, these treatments are marred by one of the key limitations i.e. cornea tissue shortage. Worldwide, in 2013,

283,530 corneas were procured and out of these only 184,576 cornea transplantations were done. About 35% of these corneas were non-suitable for transplantation purposes.[32] According to the recent Eye Bank Association of America report, in 2016, 136,318 corneas were collected from donors and out of these 73,020 were used for transplantation purposes with a majority used for PK (46%) and EK (39%) related surgeries. About 93% of EK transplants and 3% of PK transplants were due to FED; however, the number is low in PK as the cause of 43% of PK surgeries were unknown. It can be estimated that 46.4% of these corneas were unused and out of this 33% were unfit for transplantation.[73] The availability of healthy corneal tissue is further worsened by logistics, cultural, and technical issues.[74] Across the world, it has been estimated that 53% of the patients don't have access to healthy corneas indicating the severity of cornea shortage.[32]

FED is a degenerative disorder and there will likely be an increase in the number of reported FED cases due to increasing life expectancy as well as the aging population. Due to this corneal donor tissue shortage, the efforts are being pushed towards innovating new clinical therapies through tissue-engineered materials, *in vivo* regenerative therapies, cell therapies, pharmacotherapies, and many more.

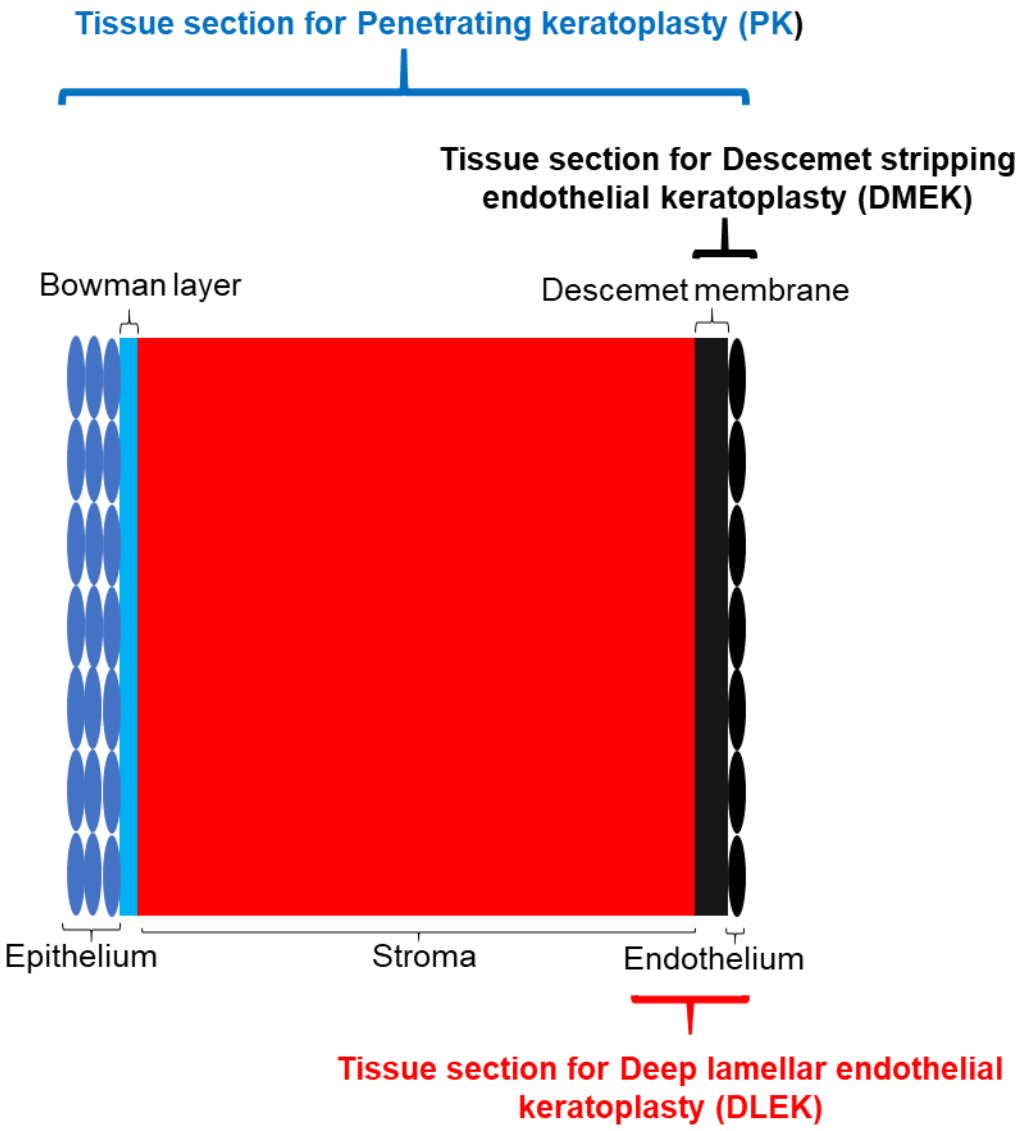

Figure 3: Corneal transplantation types and their transplanted area.

1.4 Potential future treatments for corneal endothelium dysfunction

Currently, corneal transplantation is the "gold" standard for FED. Across the world, researchers have proposed different new methods that can help to resolve this disease without much limitations and side effects. These solutions include potential pharmacological drugs, cell therapy, DM transplant, and gene therapy.[61]

Pharmacological adjuncts: This treatment method involves drug molecules that can be applied either to increase the proliferation of remaining cells or decrease the cell loss rate. Recently, ROCK inhibitors such as Y-27632 gained a lot of attention for the treatment of corneal endothelial dystrophies. Y-27632 has been demonstrated to enhance endothelial cell proliferation, adhesion, migration, and inhibiting apoptosis in the *in vitro* setup.[75, 76] Furthermore, in animal studies, some of these effects are replicated such as enhanced cell proliferation and migration.[77] It has been proposed that Y-27632 acts through P27 and cyclin-D via the PI-3 pathway.[78] In human patients, when this drug is applied topically to corneal endothelial injured patients, there was an improvement in the endothelial cell count as well as wound healing.[77]

Antioxidants might increase the longevity of endothelial cells in the FED's toxic environment. As observed in different studies, oxidative damages play a significant role in FED. In preliminary studies, the application of anti-oxidative agents such as mefenamic acid, L-ascorbic acid 2-phosphate, and oxotremorine helped in cell survival under severe oxidative stress.[79, 80]

Although, these results are encouraging, the therapeutic effects of these drugs have yet to be evaluated in clinical trials. The treatment done on patients using Y-27632 involved a small cohort (n=4). In addition, there are also contrasting results obtained from other studies where Y-27632 didn't induce cell proliferation in human cells.[76] Furthermore, the FED DM is filled with guttatas. However, these studies were done on flat substrates which did not represent the FED toxic environment and its diseased DM.

Descemet membrane transplant: Endothelial surgeries for FED involved removal of diseased DM and its guttatas. In contrast, DM stripping does not provide a suitable environment for endothelial cell layer regeneration as it has been shown that the endothelial cell migration is slower on the stromal surface.[81] However, decellularized DM transplant enhanced cell proliferation and

migration in rabbits.[82] In addition, it has been proposed that acellular biomaterials like hyaluronic acid-based materials can also be utilized for transplant.[61] It will be helpful to overcome the donor tissue shortage using cost-effective and widely available biomaterials.

Cell therapy: The above-mentioned therapies assume that healthy endothelial cells are present in the eye during FED treatment. However, in severe FED situations, it might not be the case. Hence, the transplant of the healthy endothelial cell layer might be an optimal solution. During the past two decades, a lot of improvement has been done to proliferate endothelial cells and keeping their function intact using specific culture medium, supplements, and ECM coating.[83] There are two major strategies used for cell therapy: carrier-free and carrier-based. In the carrier-free approach, cells or a cell layer is transplanted in the patient's cornea. One of the ways that cells can be transplanted into the cornea is through intracameral cell injections. In this approach, cells are cultured *in vitro* and injected into the anterior chamber of the eye. This approach has been reported to augment cell proliferation, cell monolayer formation, and restoration of corneal transparency in different species such as rabbit, monkey, and feline.[84, 85] However, human corneal endothelial cells have attenuated proliferation in comparison to other non-human species which can limit the success of this therapy. The second method utilizes cell culture on materials that can alter cell adhesion depending on an external cue. One such widely studied material is Poly(N-isopropyl acrylamide) (PNIPAAm), a well-known thermosensitive material. This material possesses a reversible hydrophilic/hydrophobic state upon changing the temperature from its lower critical solution temperature (LCST), i.e. 32°C.[86] This property directly affects its solubility in aqueous solution as it becomes insoluble when the temperature is above its LCST. Several studies are utilizing this property for corneal endothelial cell monolayer formation for transplantation purposes.[87, 88] In this method, corneal endothelial cells are cultured on the PNIPAAm based

substrates at 37°C to form a functional monolayer and the cell layer is detached from the substrate by lowering the temperature from the polymer LCST. This detached and viable monolayer can be transplanted into the cornea. Although, the cell sheet form is quite intact, the cell layer is quite thin, fragile, and difficult to handle which poses a great risk during transplantation.

The second strategy for cell therapy is similar to EK. In this strategy, cells are cultured on biological or synthetic biomimetic substrates to form a cell monolayer. After monolayer formation, this whole graft can be transplanted to DM-stripped cornea. In this method, properties of the substrate are quite important as it should be: able to adhere to corneal endothelial cells; biocompatible; transparent; mechanically strong; to facilitate diffusion between endothelial and aqueous humor; and be resistant to biodegradation. Different materials such as gelatin, chitosan, GelMA, silk, Poly-ε-lysine based hydrogels, collagen, and many more have been studied to understand the behavior of corneal endothelial cells on these substrates.[89-92] This approach overcomes the limitation of endothelial cell loss during corneal transplantation as the number of cells on the substrate can be controlled. These studies mostly focused on proliferation, monolayer formation, material characterization, and functional marker expression. However, these studies have yet to characterize the effective ability for passive diffusion, biointegration, absence of optical aberrations, and long-term survival of the graft or the ability to replace with native DM.

Gene therapy: During FED disease progression, there are many mutations observed throughout different cases. Among them, TCF4 trinucleotide repeat expansion is the most common one. Gene therapies used for other tri repeat expansion diseases such as Huntingtin disease, and myotonic dystrophy might also be applicable for FED.[61] There are many modalities of gene therapies, however, antisense oligonucleotide-based therapeutics are mostly researched for the treatment of these diseases. This therapy provides steric blockage by binding to pre-RNA

molecules which mask the repeats from splicing machinery. This masking helps to produce non-pathological RNA without any mutated repeats.[93] Similarly, this therapy can also be modified to also induce degradation of the pre-mRNA molecule through endogenous RNAse-H.[94] These types of gene therapies can be applied to reverse the effects of genetic mutations in FED. However, FED patients are diagnosed with different genetic mutations and a single treatment might not be possible without knowing the exact genetic mutations in a FED patient. Furthermore, the short term and long-term effects of these treatments in the ocular environment as well as the efficacy of these solutions in FED patients have yet to be studied.[61]

Overall, these wide varieties of potential FED treatments can be easy to apply, cost-effective, readily available, efficient over the current corneal transplantation treatment. However, the two therapies that are currently developing i.e. pharmacological and cell therapy have also their inherent limitations. In addition, there is a lack of data on these therapies in the native environment. The presence of guttatas is one of the key characteristics of FED and the effect of these features on the efficacy of these therapies has yet to be studied.[61]

1.5 Effect of ECM topographical cues and stiffness on the corneal endothelial cells

Biophysical cues such as surface topography and substrate stiffness mediate different cell functions such as cell proliferation, cell differentiation, cell migration, cell adhesion, and many more.[95-97] Endothelial cells interact with DM which is the potential source of biophysical cues.[98] DM is comprised of interwoven mesh fibers and pores and these surface topographies are in the nanometer range. Micro and nano-topographies can induce corneal endothelial cell proliferation.[99-101] Different types of topographies on Polydimethylsiloxane (PDMS) have been tested using bovine corneal endothelial cells.[101] Among these topographies, micro and nano pillars increase

cell density and cell area. Cells cultured on these pillars have a coefficient of variation of the area comparable to healthy endothelium and have a higher density of microvilli structures and upregulation of Na^+/K^+-ATPase associated with endothelial pump function. In addition, human corneal endothelial cells seeded on micro and nano pillars had improved proliferation rate, cell area, and tight junction formation.[89, 100] These pillars also enhance the impact of extracellular matrix biochemical cues on corneal endothelial monolayer formation by decreasing cell area and increasing tight junction formation.[99]

Substrate stiffness also plays a significant role in mediating cell function.[97, 102] However, human DM stiffness measurements is quite controversial in the literature.[14] The reported measurements range from 50 kPa to 2.5 MPa. During FED, the DM stiffness changes, and it is reported to be decreased in areas where guttata reside (from 1.8 MPa to 1 MPa).[103] However, this phenomenon is yet to be confirmed by other studies. Substrate stiffness changes also impact corneal endothelial cell behavior.[104] Corneal endothelial cells have been cultured on various biomaterials possessing different biochemical and biomechanical properties. Palchesko et al. analyzed the impact of substrate stiffness changes on corneal endothelial cells. In this study, they seeded bovine corneal endothelial cells observed that bovine corneal endothelial cells have a higher proliferation, polygonal morphology, and tight junction formation on 50 kPa PDMS gels in comparison to stiff or softer substrates.[104]

1.6 Cell tension and ROCK signaling in apoptosis

During FED, endothelial cell loss occurs, and it has been shown that this loss is due to cell apoptosis.[105-107] In different studies, endothelial cells in FED patient's cornea buttons were TUNEL positive (cells were stained positive for TUNEL staining), indicating late stage apoptosis; while it was almost absent in healthy cornea buttons. Furthermore, it is observed that an average

2.65% of endothelial cells were stained positive for cell apoptosis as compared to 0.23% in healthy cells.[105]

Apoptosis is a form of programmed cell death involving genetically determined cell elimination.[108] This process plays an important role during animal development, homeostasis to maintain healthy population, and defense mechanisms when cells are damaged by external agents. The apoptosis can occur in a single cell or it can involve small cluster of cells. During early apoptotic stage, cells start to shrink and pyknosis (chromatin condensation) starts to appear. These cells become round or oval shape. At later stages, karyorrhexis, a process of fragmentation of nucleus sets in which further leads to cell fragmentation. After these steps, budding process starts in which cell fragments separates into apoptotic bodies. These cytoplasmic apoptotic bodies contain cell contents such as tightly packed organelles and genetic material. Meanwhile, during this process, organelles are encapsulated with plasma membrane to maintain their integrity. Later, these apoptotic bodies are phagocytosed by immune cells such as parenchymal cells, neoplastic cells, or macrophages. During this whole process, there is no inflammatory response as the cells are quickly phagocytosed to prevent secondary necrosis and cell contents are not released in the surrounding environment.

Plasma membrane and cell cortex play an important role in cell apoptosis such as the formation of spherical membrane evaginations or blebbing. Blebbing is a crucial step during apoptosis, and it is regulated by mechanical as well as biochemical cues.[109] Blebs are formed when disruption of cell-substrate and plasma membrane-cytoskeletal interaction is disrupted. Therefore, cells become unable to sustain the fluid pressure created by the inward contraction of actin cytoskeleton.[110, 111] Plasma membrane tension is an accumulative effect of transverse and lateral forces on the membrane such as hydrostatic pressure in the lipid bilayer and tension caused by membrane-

cytoskeletal adhesion.[112] The typical membrane tension range for a cell is in the range of 0.01 to 0.04 mN/m. However, during bleb formation, after the reduction of membrane-cytoskeletal adhesion tension resulting cell membrane tension is four-fold lower than the tension in a healthy cell.[113] The remaining force in a bleb is mainly due to increase hydrostatic pressure. These studies indicate that cell cortex forces are the primary responsible for cell membrane tension as well as bleb formation.

Cell cortex lies below the cell membrane and it is composed of actin, myosin, and associated proteins in a thin meshwork structure.[110] Active myosin motors regulate actin filaments polymerization/depolymerization rate causing cytoplasm to contract and relax. This mechanism generates two type of forces i.e. cortical tension, which is restricted to forces experienced by cell elements such as plasma membrane and the other force is adhesion force exerted through cell-substrate adhesion complexes.[114] During apoptosis, cells start detaching from the surface through rearrangement and cleave of focal adhesion complexes attached to actin stress fibers occurs through caspase mediate mechanism. Simultaneously, reorganization of actin occurs at peripheral ring as actin stress fibers are lost. Later, actin associated proteins mediate the contraction of cortical actin ring leading to bleb formation which later segregate to form apoptotic bodies.[115] Furthermore, these cytoskeletal dynamics are regulated by Rho associated protein kinases (ROCK) signaling pathways.[116]

ROCK proteins specifically ROCK1 and ROCK2 are involved in regulating cell apoptosis in multiple cellular systems.[117, 118] Depending on the system, these proteins can either promote cell survival or cell apoptosis.[116, 119] However, in corneal endothelial cells, ROCK inhibition has been shown to promote cell proliferation and cell survival during injury suggesting the role of ROCK in mediating cell apoptosis.[75, 76] During apoptosis, ROCK proteins are cleaved by Caspase

dependent (Caspase-2 or Caspase-3) or independent pathways leading to removal of its autoinhibitory C-terminal domain.[120] This cleavage results in ROCK activation which leads to increase in myosin light chain (MLC) phosphorylation. Increase in MLC phosphorylation induces cortex contractility which further causes bleb formation as well as it can induce loss of cell adherence.[116, 121] Furthermore, ROCK also facilitates DNA redistribution into apoptotic bodies and blebs as well as fragmentation of organelles such as Golgi apparatus.[120, 122] ROCK mediated apoptosis mechanisms can be categorized into two different forms based on apoptotic pathways i.e. extrinsic and intrinsic. In an example of an extrinsic pathway, ROCK mediates apoptosis through Fas cell surface death receptor-ezrin-radixin-moesin (FAS-ERM) complex in jurkat cells.[123] Upon receiving external cue, ROCK proteins phosphorylate ezrin and moesin, which later form a complex with FAS, a transmembrane protein, leading to its attachment with the cytoskeleton and forming aggregates. These aggregates interact with Fas Associated Via Death Domain (FADD) and procaspases such as procaspase-8 inducing the activation of caspase-8 which causes the induction of cell apoptosis. Meanwhile, in one example of the intrinsic pathway, ROCK phosphorylate Phosphatase and tensin homolog (PTEN) which causes Protein kinase B (Akt) pathway inactivation, a pathway associated with cell survival.[124] Hence, depending on cell type and stimuli, ROCK can act through different substrates to induce cell apoptosis including phosphorylated myosin light chain (pMLC) mediated cytoskeletal contraction.

1.7 Synthetic guttata model

Kocaba et al. observed the phenotypes of cells seeded on native FED DM.[60] These membranes varied in their structures and diseased stages. HCEnC-21T cells seeded on FED DM had less percentage of cell covered area as well as the density was lower. In addition, they possessed an irregular morphology along with the incomplete formation of tight junctions. Furthermore, DM

consisting large guttatas (most likely advanced disease stage) had higher upregulation of EMT related genes αSMA, N-cadherin, and Snail in comparison to mid or small guttata (most likely early disease stage).[60] In addition, NOX-4, oxidative stress molecule was also upregulated in the DM containing medium and larger guttatas. On FED DM, cells were apoptotic and were largely located in proximity to guttata.[60]

Rizwan et al. analyzed the dimensions of guttatas in FED patients as well as previously published data.[28] Guttatas were in the range of 3-25 μm in height, 6-70 μm in width, and 3- 240 μm in spacing depending on the diseased stage and their shape closely resembled like pillars or dome like structures. Hence, they developed synthetic guttata (s-guttata) model with the pillar dimensions in the range of 5-20 μm in height, 10-40 μm width, and 20-120 μm center to center spacing to represent the early and late stage guttatas. Furthermore, they tested the impact of guttatas on both primary human corneal endothelial cells and human corneal endothelial cell line (B4G12).

B4G12 cells are immortalized and proliferative cells derived from adult human corneal endothelial cells with an average generation time of 62.26 +/- 14.5 h.[125] B4G12 closely resemble primary endothelial cells in many aspects such as monolayer formation, collagen IV expression, formations of cell junctions (ZO-1, connexin-43, and occludin expression), and Na^+/K^+-ATPase expression.[99, 125] In addition, B4G12 cells share 83% of the total expressed genes with *ex vivo* human corneal endothelial cells.[126] However, out of 138 *ex vivo* human corneal endothelial cells specific genes, only 28% are expressed in B4G12.

In the s-guttata model, s-guttatas with 20 μm heights along with a diameter greater than 20 μm created the maximum disruption of the monolayer and tight junction formation in both primary human corneal endothelial cells and human corneal endothelial cell line (B4G12). However,

primary cells were more affected by 40 μm diameter as decreasing the height did not improve monolayer formation. In addition, these patterns also affected the primary and B4G12 cell migration behavior such as migration direction and Euclidean distance.

2. Hypothesis and Objectives

Currently, the only available treatment for FED is corneal transplantation. The shortage of healthy cornea along with post-surgery complications poses as limiting steps. The discovery of potential cell and pharmacological therapies for FED will overcome these limitations and meet the needs of FED patients. In future, these therapies can also be tailored according to an individual's basis. However, the effectiveness of these therapies in the presence of different dimensions of guttatas has not yet been established. The increasing presence of guttatas during FED is correlated with corneal endothelial cell loss.[55] However, it is not yet clear that how the presence of guttatas affect the behavior of corneal endothelial cells. The creation of s-guttata FED disease model might provide answer to these questions.[28] Previous study from our lab indicated that varying dimensions, density, and spacing greatly affected the monolayer structure as well as migration behavior. This study suggested that s-guttata structures might act as a mechanical cue and can affect corneal endothelial cell behavior. In addition, the effect of stiffness has been documented on corneal endothelial cells.[104] Hence, these observations led to formulate the hypothesis that s-guttata structures and DM stiffness play a role in corneal endothelial cell apoptosis contributing to the FED disease progression with the following three objectives:

1) Identification of the effect of s-guttata size in the corneal endothelial cell apoptosis.
2) Study the potential mechanisms of cell apoptosis on these s-guttatas through cytoskeletal analysis.
3) Study the cumulative effect of stiffness and topography on corneal endothelial cells.

The first two objectives will be covered in chapter 3 describing the studies and data analysis. However, objective 3 will be covered in chapter 4 consisting of preliminary studies to achieve this objective.

3. Synthetic *in vitro* model for FED studies and regenerative therapies

3.1 Introduction

Corneal endothelium, posterior-most cell layer in the cornea, plays an important role in corneal transparency by maintaining stromal dehydration.[17] However, during Fuchs' endothelial dystrophy (FED), this function is disrupted and rest of cornea become excessively hydrated.[21, 28, 30] This phenotype is due to the apoptosis of corneal endothelial cells during FED progression.[30] One of the commonly observed clinical hallmarks of FED is the deposition of abnormal collagen excrescences, also known as guttata, on the DM. These guttatas appear at the center during its onset and move towards the peripheral side as the disease progresses. Guttata's density is present in a gradient form where it is highest in the center and lowest at the peripheral area.[28] The presence of guttatas during FED progression is correlated to the endothelial cell density; as guttatas presence increase, the endothelial cell density decreases.[55, 56] However, the effect of these guttatas in FED is largely unknown.

Cornea transplantation is the only treatment available for FED. However, there is a severe shortage of healthy corneas in the world.[32] Currently, pharmacotherapy and cell injection therapy are being developed to treat FED disease.[27, 75, 77, 84, 85, 127] During the application of therapies, diseased DM is kept intact and guttatas are still present. The presence of these guttatas during these therapies might affect their efficiency. During FED, these guttatas are present in micro-pillar like structures with varying height, spacing, and diameter.[28] It is also not completely clear how the dimension of these guttatas affect the corneal endothelial cells.

Previously, our lab developed the s-guttata model to understand the impact of these guttatas on cell migration and monolayer formation.[28] Hence, I used this system to understand the apoptotic behavior of corneal endothelial cells. In this chapter, apoptotic marker expression in cell injection therapy like conditions is examined. Along with early stage apoptotic marker expression, cells

present in vicinity to these s-guttatas also express late stage apoptotic marker expression. In addition, cells adjacent to s-guttatas also possess higher cytoplasmic stress. Collectively, this chapter reveals the potential of s-guttatas to induce cell apoptosis.

3.2 Materials and Methods

3.2.1 Cell Culture

Human corneal endothelial cells (B4G12, DSMZ, Germany) were maintained in 10 cm dish in the culture media containing 10% Fetal Bovine Serum (FBS, Gibco) and 1% Penicillin-Streptomycin (Gibco). Cells were incubated in the incubator (5% CO_2 and 37°C) and media was changed every other day until cells become confluent. For cell propagation and experiments, cells were passaged using 0.25% trypsin (Gibco) and seeded on substrates with appropriate cell density.

3.2.2 Polystyrene and Polydimethylsiloxane (PDMS) synthetic molds fabrication

PDMS was mixed with curing agent in 10:1 ratio and bubbles were removed using vacuum desiccator for 30 mins. Later, PDMS was spread on the silicon wafer molds (the silicon wafers design and processing has been described in Rizwan et al. [28]; the silicon wafers were obtained from Dr. Muhammad Rizwan) and incubated in a vacuum desiccator for 1h. After removal of all trapped air, PDMS with silicon mold was incubated in the oven for polymerization at 60°C for overnight. Next day, polymerized PDMS molds were detached from the silicon wafer. The following s-guttatas were fabricated in the following dimensions:

Diameter (µm)	Spacing between s-guttatas (µm)	Height (µm)	Assigned name
20	20	20	20x20x20
20	40	20	20x40x20
40	40	20	40x40x20
40	80	20	40x80x20

Table 1: Dimensions of fabricated s-guttatas

Similarly, PDMS molds were fabricated to create wells (inverse replica of pillars). These molds were plasma treated for 60s at 80% O2 gas and 60 Watts (Zepto, Diener). After treatment, these molds were coated with (1H,1H,2H,2H)-perfluorodecyl trichlorosilane (FDTS, Sigma), an anti-stiction layer. To remove the excess reagent, PDMS molds were replicated at least three more times. After these steps, these molds acted as the master molds for polystyrene (PS) substrate fabrication.

PS pieces (2cm x 2cm) were cut from the large polystyrene sheet (Goodfellow Corporation US) and rinsed with ethanol and air dried. These pieces were embossed with patterned PDMS molds at 250°C and 0.3–0.5 MPa for 90s using heat embossing.[28] After 90s, the system is shut off and samples were left on the stage for another 10 mins to cool down. Unpatterned PDMS molds were used as masters to prepare control PS samples. For defects detection, samples were visualized under the bright field microscope and LEXT OLS5000 3D measuring laser microscope (Olympus).

3.2.3 Cell seeding on patterned samples

Patterned and unpatterned PS samples were cleaned with ethanol, air dried, and plasma-treated 60s at 80% O2 gas and 60 Watts (Zepto, Diener). After plasma treatment, these samples were sterilized for an hour under the UV light in a biosafety cabinet. Cells were seeded directly on

the samples at a density of 300,000 cells/cm^2 (300k/cm^2) or 100,000 cells/cm^2 (100k/cm^2). Cells were cultured for 24h and 48h before processing.

3.2.4 Annexin V staining and quantification

Cell media was removed from the samples and cells were washed two times with 1x phosphate-buffered saline (PBS). Samples were incubated for 15 mins in dark in 100µl annexin V and propidium iodide (PI) solution (solvent: annexin binding buffer (10 mM HEPES, 140 mM NaCl, and 2.5 mM CaCl2 in PBS, pH 7.4), 25µl annexin V dye (A13201, ThermoFisher), and 2.5µl PI dye (100 µg/ml, P1304MP, ThermoFisher)). After incubation, cells were washed twice with annexin binding buffer and fixed with 4% PFA containing 10 mM HEPES, 140 mM NaCl, and 2.5 mM $CaCl_2$ for 15 mins. Further, cells were washed twice with annexin binding buffer and incubated in DAPI dye (1:1000, Invitrogen, USA) for 30 mins. Cells were washed twice and incubated in annexin binding buffer. Samples were imaged using Zeiss immunofluorescence microscope at 10x magnification using z-stack option at 2 µm intervals (starting from basal plane to apical plane of s-guttatas). Images were analyzed using Fiji (ImageJ) and all images in a single channel were merged using z-project option (maximum intensity projection). Further, brightness and contrast adjustments were made using Fiji software.

Fiji was used for cell quantification using the raw images. The population was quantified by manually adjusting the threshold to remove background from different channels and the stained cells were measured using “analyze particle” option.

3.2.5 TUNEL staining and quantification

Cell media was removed, and cells were washed with 1xPBS; then cells were fixed with 4% PFA. After fixation, cells were permeabilized with 0.2% Triton (in PBS) for 5 mins at room temperature. Cells were washed twice with 1x PBS and incubated in equilibration buffer at room

temperature for 10 minutes. Cells were further incubated in rTDT solution (equilibration buffer, Nucleotide Mix, and rTDT enzyme) at 37ºC for 1h in dark conditions as per the manufacturer's protocol (G3250, Promega). Later, this reaction was terminated by incubating samples in 2x SSC buffer for 15 mins at room temperature. Cells were washed thrice with 1x PBS and samples were incubated in DAPI dye (1:1000, Invitrogen, USA) for 30 mins. Cells were washed with 1x PBS and stored in 1x PBS buffer.

Samples were imaged using Zeiss immunofluorescence microscope at 10x magnification using the z-stack option at 2 μm intervals (starting from basal plane to apical plane of s-guttatas). Images were analyzed using Fiji (ImageJ) and all images in a single channel were merged using the z-project option (maximum intensity projection). Further, brightness and contrast adjustments were made using this software. Fiji was used for cell quantification using raw images. The population was quantified by manually adjusting the threshold to remove background from different channels and the stained cells were measured using the "analyze particle" option.

3.2.6 Cytoskeletal staining

Cells were washed 1x PBS and fixed with 4% PFA for 15 mins. Cells were permeabilized and blocked in the solution containing 0.1% Triton-X, 10% goat serum, and 1x PBS for 1h at room temperature. After blocking, cells were incubated in Phosphorylated myosin light chain (pMLC) primary antibody (1:50, 3671, NEB) for 1h at room temperature and cells were washed 1x PBS. For secondary antibody incubation, cells were incubated with the anti-rabbit 448 conjugate (1:500, Invitrogen) for 1h at room temperature. Further, cells were incubated with DAPI (1:1000, Invitrogen) and phalloidin (1:500, Invitrogen) for 30 mins. Samples were stored in 1x PBS for imaging. Samples were imaged using Zeiss immunofluorescence microscope at 20x and 40x magnification using the z-stack option at 2 μm intervals (starting from basal plane to apical plane

of s-guttatas). Images were analyzed using Fiji (ImageJ) and all images in a single channel were merged using the z-project option (maximum intensity projection). Further, brightness and contrast adjustments were made using this software.

3.2.7 Cell location quantification

Fiji was used for cell quantification purposes using the raw images. Images were stacked using z-project option (maximum intensity projection). Bright field image threshold was adjusted to remove the background so only s-guttatas remain. Using the "create selection" and "create mask" option, a mask of s-guttata patterns were created for each individual image.

For PI, annexin V, and TUNEL stacked images, the threshold was manually adjusted to remove the background. Using the analyze particle option, an outline for all the positive cells was created and the mask was overlapped with this outline. Later, the cells touching the s-guttata boundary and the cells which were dispersed in between s-guttatas were manually counted.

3.2.8 Statistics

For all the samples, one-way ANOVA with Dunnet's test was applied to determine the statistical significance with respect to control. TUNEL and annexin V experiments had at least 3 biological replicates and 2 technical replicates, while pMLC studies had 2 biological replicates and 2 technical replicates. For each biological replicate, at least two images per technical replicate were analyzed and each image consisted of at least 500 cells. $p \leq 0.05$ is set as a statistical significance threshold and all data are presented as means ± SD.

3.3 Results and Discussion

3.3.1 Guttata fabrication through heat embossing

S-Guttata model was created on TCPS.[28] Unpatterned TCPS molds were embossed with patterned TCPS through heat and pressure to create surface structures on TCPS (Fig 4A). In FED, the guttatas resembled pillar like structures as well as the spacing was always <20 microns.[28] In addition, B4G12 cells are proliferative and would be able to climb the guttatas with lower heights. 20 µm height pillars acts as significant obstruction for complete cell layer formation as compared to other heights. Hence, to mimic the advanced FED disease stage, TCPS substrates consisting patterns of 20 µm height pillars with varied diameter and spacings were created (Fig 4B).

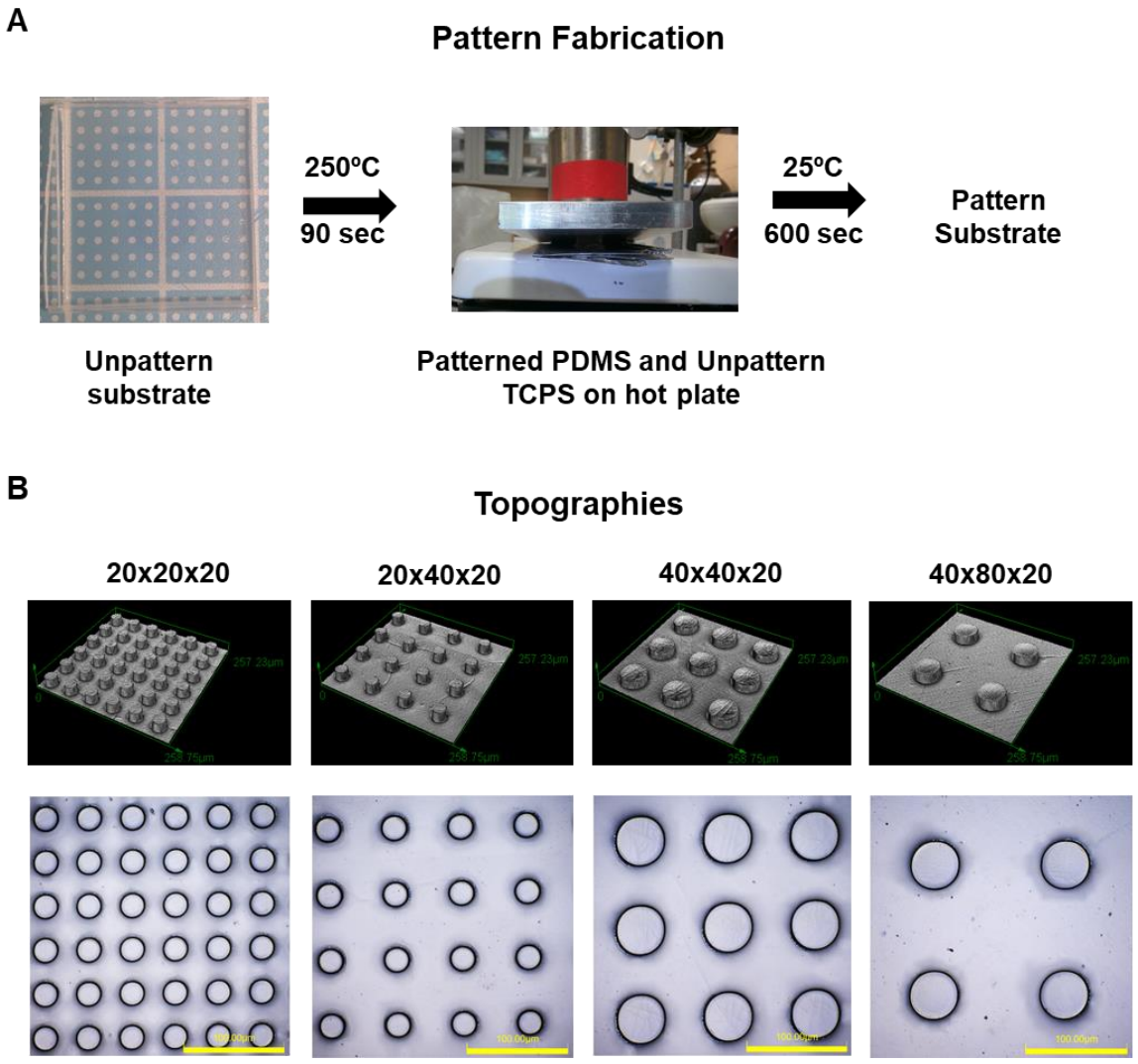

Figure 4: Guttata Fabrication on TCPS.
A) Schematic diagram of s-guttata fabrication process using hot embossing technique.
B) Representative images of patterns on TCPS with Diameter x Spacing x Height. Scale bar:100µm.

3.3.2 Early stage apoptosis in high seeding cell density

Apoptotic corneal endothelial cells are one of the phenotypes of FED.[105, 106] However, it has been unclear if guttatas play a role in cell apoptosis. To test this hypothesis, the s-guttata model was used, and cultured B4G12 cells, a human corneal endothelial cell line, on these substrates.

Using the cell therapy seeding density [128], cells were seeded at a high seeding density i.e. 300k/cm^2. These cells were stained for annexin V marker expression on Day 1 and Day 2. Unpattern TCPS was used as the negative control. Cells seeded on the TCPS substrate were completely confluent by Day 1 (Fig 5A). Through the immunofluorescence images, cells seeded on s-guttatas show higher annexin V staining Day 1. Meanwhile, PI positive cells were relatively fewer in percentage as compared to annexin V. Upon quantification, annexin V positive population on s-guttatas was significantly higher in all the patterned substrates as compared to unpatterned control (Fig 5B). However, significant difference was not observed in annexin V positive population among different s-guttata substrates. In addition, s-guttata patterns (20x20x20 and 20x40x20) had a higher PI population as compared to control; however, the percentage of dead cells was still quite low (2.7%+/-0.6% and 2.0%+/-0.9%, respectively) than annexin V positive cell population (8.6%+/-1.5% and 7.8%+/-1.4%, respectively).

Similarly, on Day 2, cells on s-guttatas showed a higher annexin V population, but not much dead cells were observed as seen through PI staining (Fig 6A). When quantified, annexin V positive population on s-guttatas were significantly higher than control (Fig 6B). In contrast to Day 1, all s-guttatas had a significant higher PI percentage and the PI positive population percentage (2.9%+/-0.6%) was still smaller than annexin positive population (8.4%+/-1.6%). In addition, data on both days have a relatively same percentage of annexin V positive population, and a slightly higher increment in PI positive population was also observed.

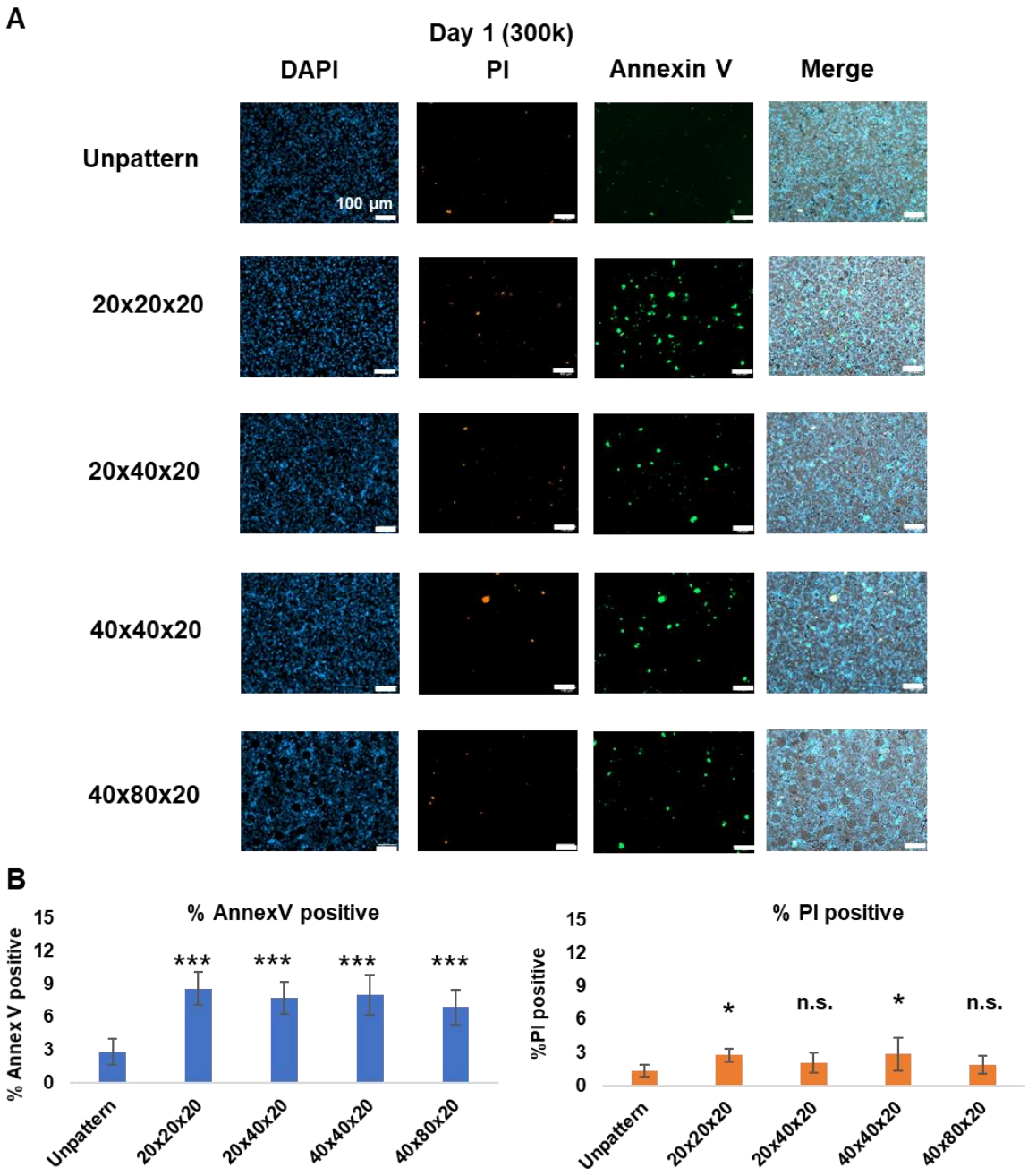

Figure 5: B4G12 on s-guttata show higher early stage apoptotic marker expression on Day 1 at higher cell density

A) Representative IF images of annexin V and PI staining of corneal endothelial cells seeded on different s-guttata substrates. Scale bar: 100µm

*B) Graphs representing annexin V positive and PI positive cell population on different s-guttata patterns. *P < 0.05; **P < 0.01; ***P < 0.001*

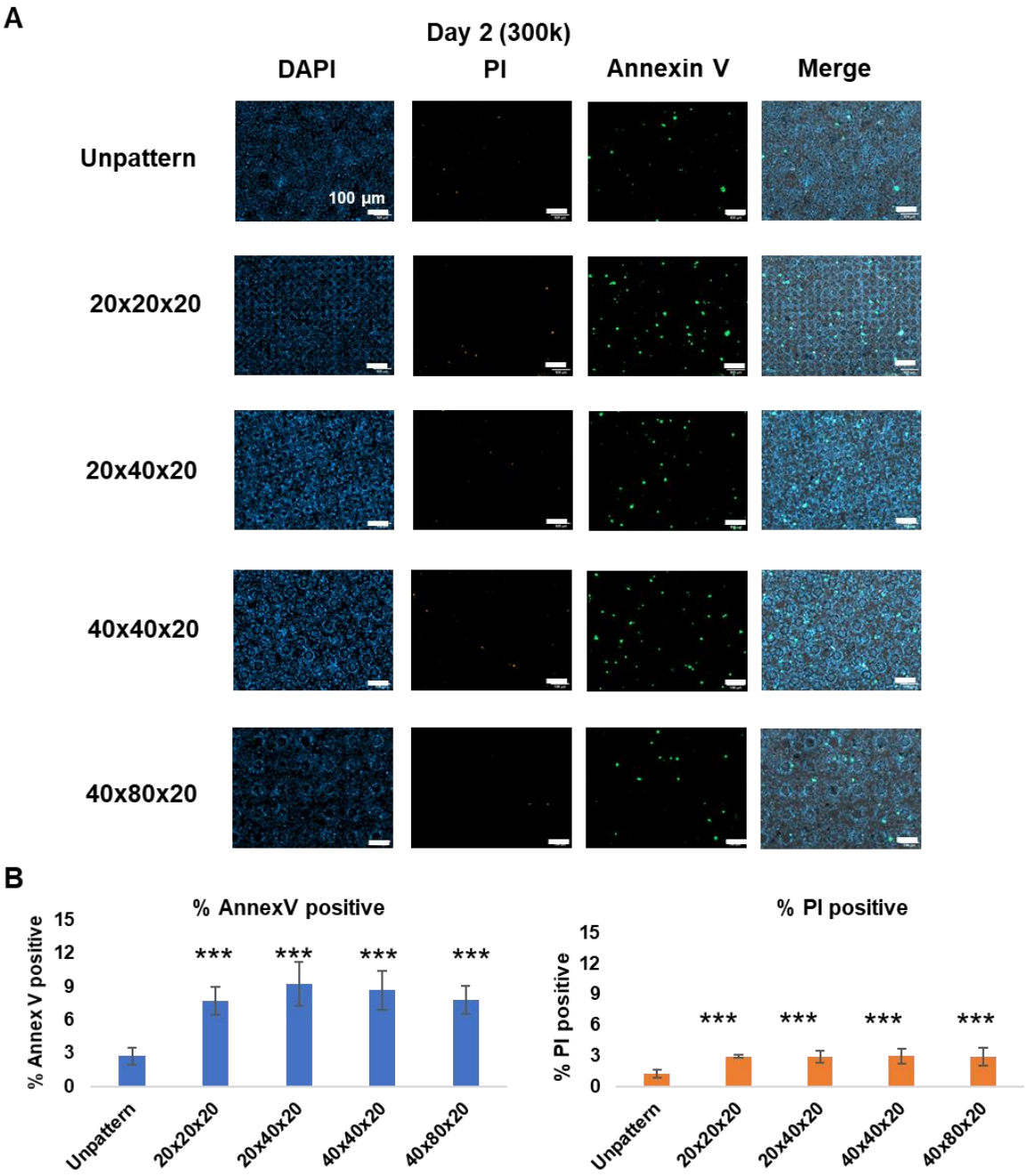

Figure 6: B4G12 on s-guttata show higher early stage apoptotic marker expression on Day 2 at higher cell density

A) Representative IF images of annexin V and PI staining of corneal endothelial cells seeded on different s-guttata substrates. Scale bar: 100µm

*B) Graphs representing annexin V positive and PI positive cell population on different s-guttata patterns. *P < 0.05; **P < 0.01; ***P < 0.001*

3.3.3 Early stage apoptosis in low cell density

Unpattern TCPS was used as the negative control. For low density condition, a cell density of 100k/cm^2 was used as a control comparison to the 300k/cm^2. The cell apoptosis was analyzed through annexin V staining on two different days: Day 1 and Day 2. On Day 1, a relatively higher expression of annexin V was observed on the s-guttata substrates while there were relatively few cells showing PI expression in all the conditions (Fig 7A). In the merged images (cell nuclei, annexin V, PI, and bright field), annexin V positive cells appear to mostly present around s-guttatas especially in the lowest diameter and spacing s-guttata (20x20x20). When quantified, the cells expressing early stage apoptotic marker is significantly higher in patterned conditions with varying diameter and spacing as compared to the unpattern control. Meanwhile, no significant differences were observed in the PI positive population in the patterned conditions relative to unpattern substrate suggesting the similar percentage of dead cells across substrates (Fig 7B).

Similarly, on Day 2, s-guttatas appears to have relatively higher expression of annexin V positive cells (Fig 8A). Meanwhile, cells on the smaller diameter s-guttatas i.e. 20x20x20 and 20x40x20 appears to have higher annexin V expression surrounding s-guttatas. On these patterns, annexin V cells have surrounded s-guttatas in a rosette type pattern. Upon quantification, these 20x20x20 and 40x80x20 s-guttatas have significantly higher percentage of annexin V positive cells; while 20x40x20 and 40x40x20 patterns depict relatively higher percentage of annexin V positive cells as compared to unpattern control. In addition, PI analysis indicates non-significant differences in the patterns 20x20/40x20 and 40x40x20 with respect to unpattern substrate (Fig 8B). Cumulatively, these results suggest that at a low cell density, s-guttatas can induce early stage apoptosis.

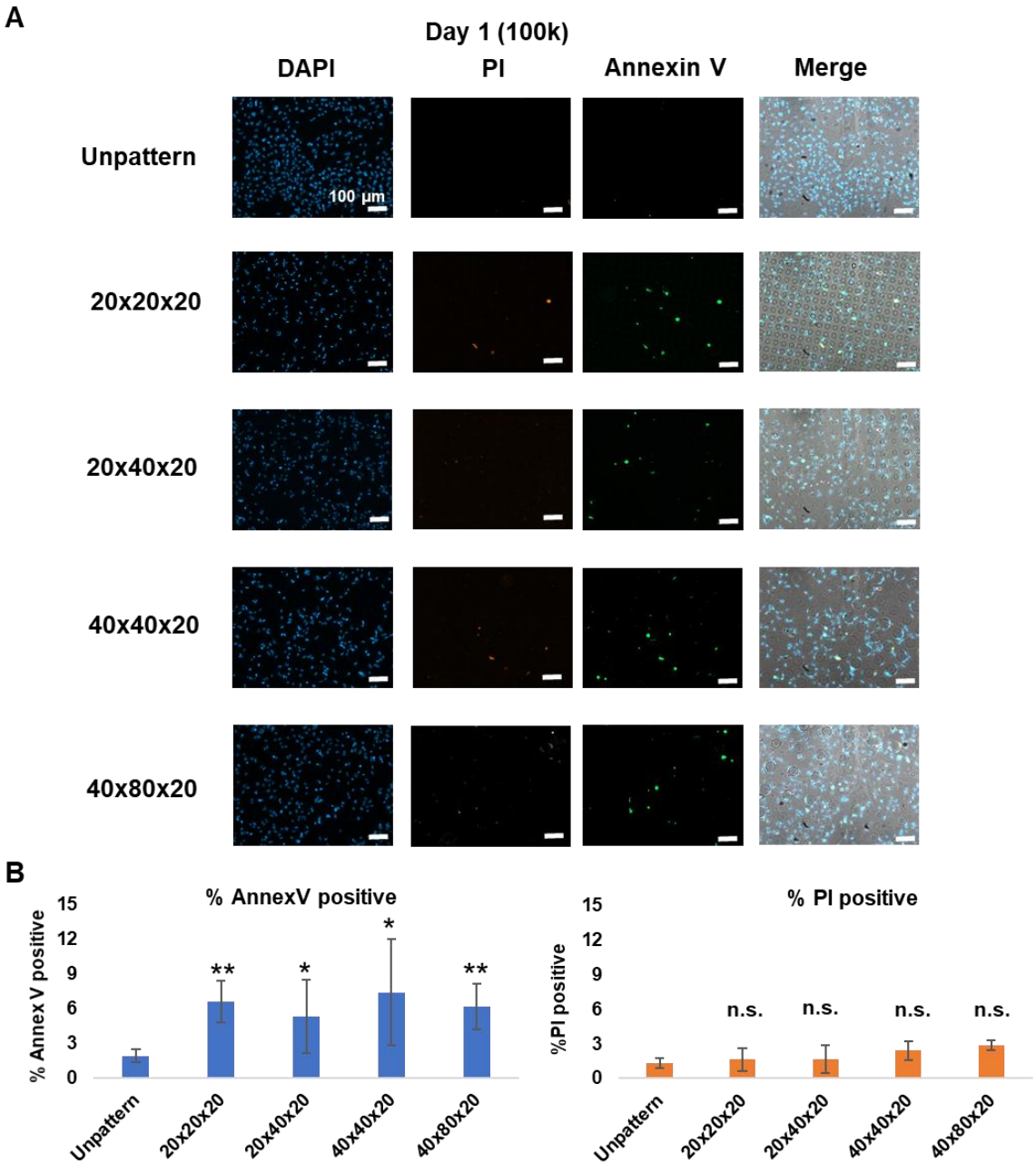

Figure 7: B4G12 cells on s-guttata show higher early stage apoptotic marker expression on Day 1 at lower cell density

A) Representative IF images of annexin V and PI staining of corneal endothelial cells seeded on different s-guttata substrates. Scale bar: 100µm
*B) Graphs representing annexin V positive and PI positive cell population on different s-guttata patterns. *P < 0.05; **P < 0.01; ***P < 0.001*

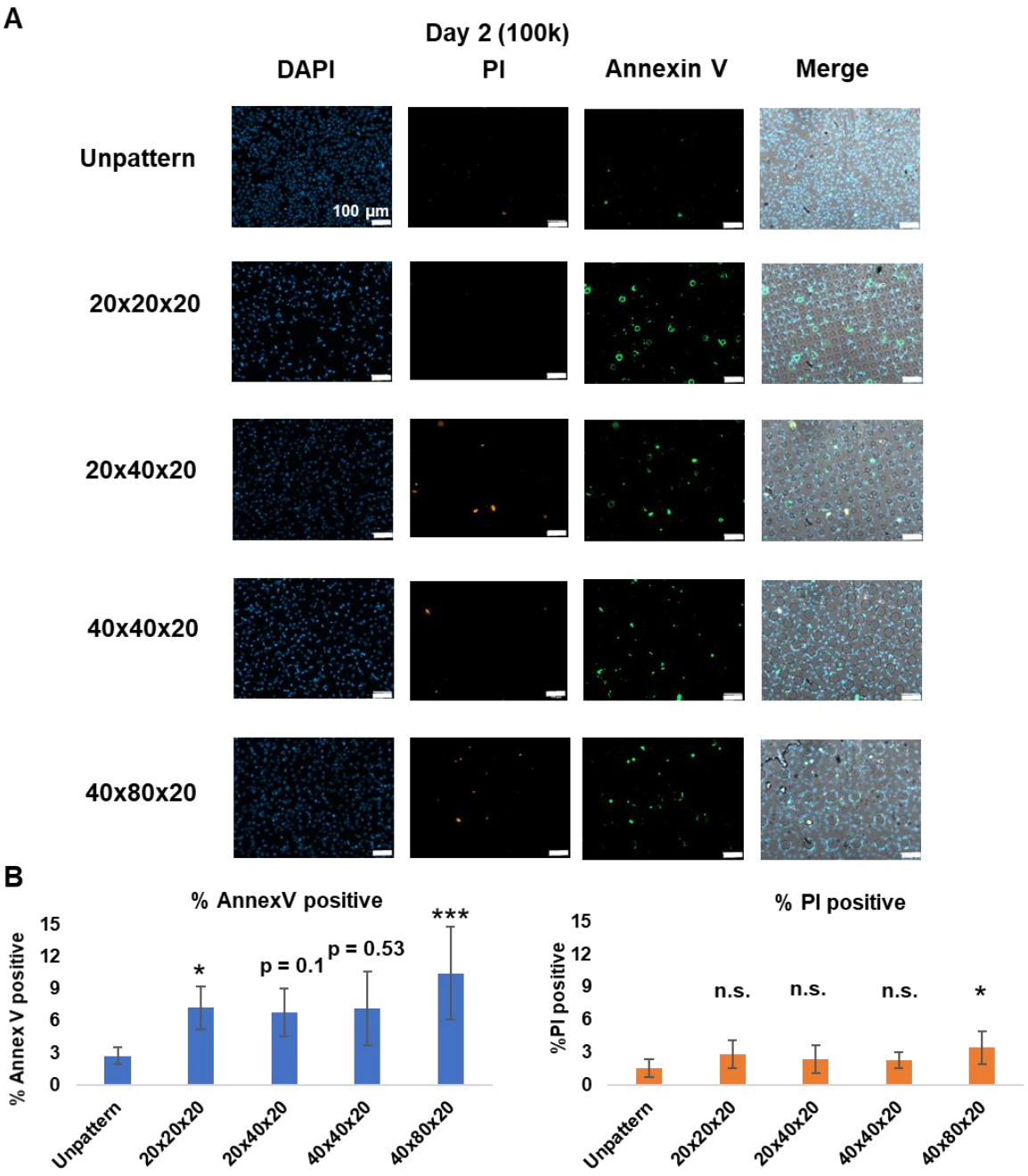

Figure 8: B4G12 on s-guttata show higher early stage apoptotic marker expression on Day 2 at lower cell density

A) Representative IF images of annexin V and PI staining of corneal endothelial cells seeded on different s-guttata substrates. Scale bar: 100µm

*B) Graphs representing annexin V positive and PI positive cell population on different s-guttata patterns. *P < 0.05; **P < 0.01; ***P < 0.001*

3.3.4 DNA breakage analysis in high cell density on guttatas

As from previous results, s-guttata topography had the potential to induce early stage apoptosis in cells seeded on s-guttata with both high and low seeding densities. Subsequently, whether these cells go through the late apoptotic stages such as DNA breakage were tested. Hence, the DNA breakage in these cells was examined using TUNEL assay at a high density as annexin V positive population was similar in both low and high densities. Cells population on s-guttatas appeared to show more TUNEL positive cells on both Day 1 and Day 2 (Fig 9A). However, more TUNEL positive cells presented on Day 2 as compared to Day 1. Cell population on s-guttatas had more TUNEL positive cells relative to unpatterned substrate on both days (Fig 9B). On Day 1, patterns with spacing larger than 20 μm had significantly higher TUNEL positive cells, compared to unpatterned substrate. Meanwhile, on Day 2, the percentage of TUNEL positive cells was higher in all the samples. In addition, although the TUNEL positive cell population on other patterns were relatively higher than control, specifically 40x80x20 was the only pattern with a significant increase in TUNEL positive cell percentage. In summary, cells on s-guttatas also showed late apoptosis on both days, especially patterns with spacing larger than 20 μm.

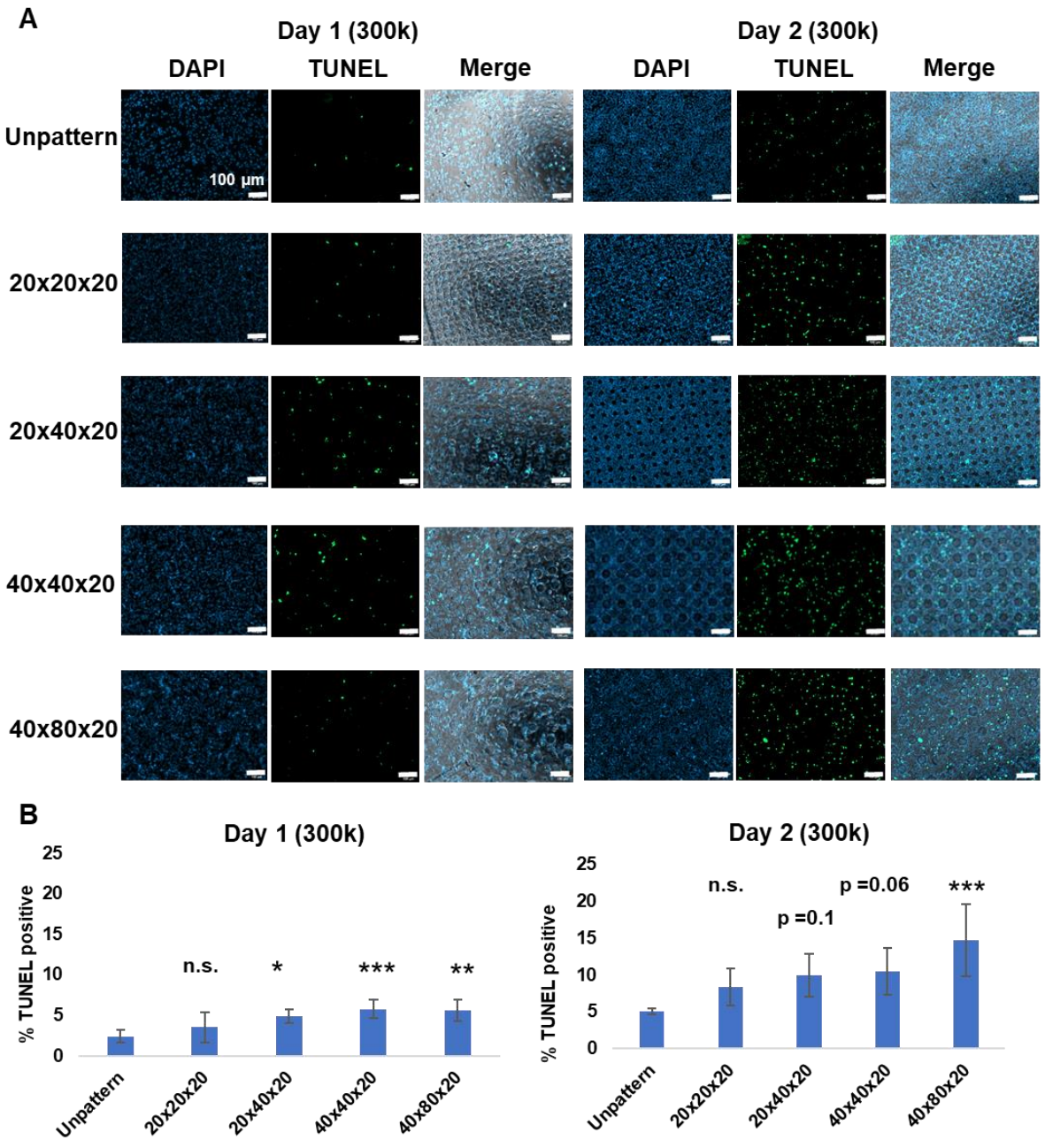

Figure 9: Guttata induces late stage apoptosis
A) Representative IF images of TUNEL staining of corneal endothelial cells seeded on different s-guttata substrates on Day 1 and Day 2. Scale bar: 100µm
*B) Graphs representing TUNEL positive cell population on different s-guttata patterns on Day 1 and Day 2. *P < 0.05; **P < 0.01; ***P < 0.001*

3.3.5 Apoptotic cells localization on s-guttatas

As s-guttatas could induce the cell apoptosis, the location of these apoptotic cells relative to the s-guttata was analyzed. On Day 1, 76.6%+/-5.8% of annexin V positive cells on 20x20x20 pattern were around s-guttatas (Fig 10A). In addition, 67.0%+/-11.0% PI positive cell population was also localized around s-guttatas in 20x20x20 patterns. However, annexin V and PI positive cell populations adjacent to s-guttatas declined in the remaining patterns. On 20x40x20 and 40x40x20 patterns, 46.8%+/-5.7% and 51.6%+/-2.2% annexin V cell populations were found around the s-guttatas, respectively. Similarly, 42.1%+/-10.4% and 47.0%+/-10.2% of PI positive cell population were found surrounding the s-guttatas on the 20x40x20 and 40x40x20 patterns, respectively. However, on the largest diameter and the largest spacing pattern i.e. 40x80x20, the lowest PI (40.8%+/-13.7%) and annexin V (32.4%+/-4.1%) positive cell populations were found around s-guttatas.

On Day 2, similar results were observed. On the 20x20x20 patterns, 78.2%+/-4.4% annexin V and 67.9%+/-9.8% PI positive cell populations were found surrounding the s-guttatas (Fig 10B). Meanwhile, on 20x40x20 pattern, 47.2%+/-7.7% annexin V and 43.7%+/-9.7% PI positive cell population were found around s-guttata. On the larger diameter patterns, 40x40x20 had 53.7%+/-8.6% and 47.9%+/-9.4% annexin V and PI positive cell populations around guttatas, respectively. However, there was a slight increase in the annexin V cell population adjacent to s-guttatas i.e. 36.8%+/-6.0% on the 40x80x20 pattern. Meanwhile, PI positive population remained constant (40.9%+/-12.3%). Similar to the annexin V results, the analysis of the TUNEL positive cell localization also showed similar trend: 70.0%+/-10.6% and 81.8%+/-4.8% TUNEL positive cells were located around 20x20x20 s-guttatas on Day 1 and Day 2, respectively (Fig 10C). Similar to annexin V, 20x40x20, 40x40x20, and 40x80x20 patterns had less %TUNEL positive cells

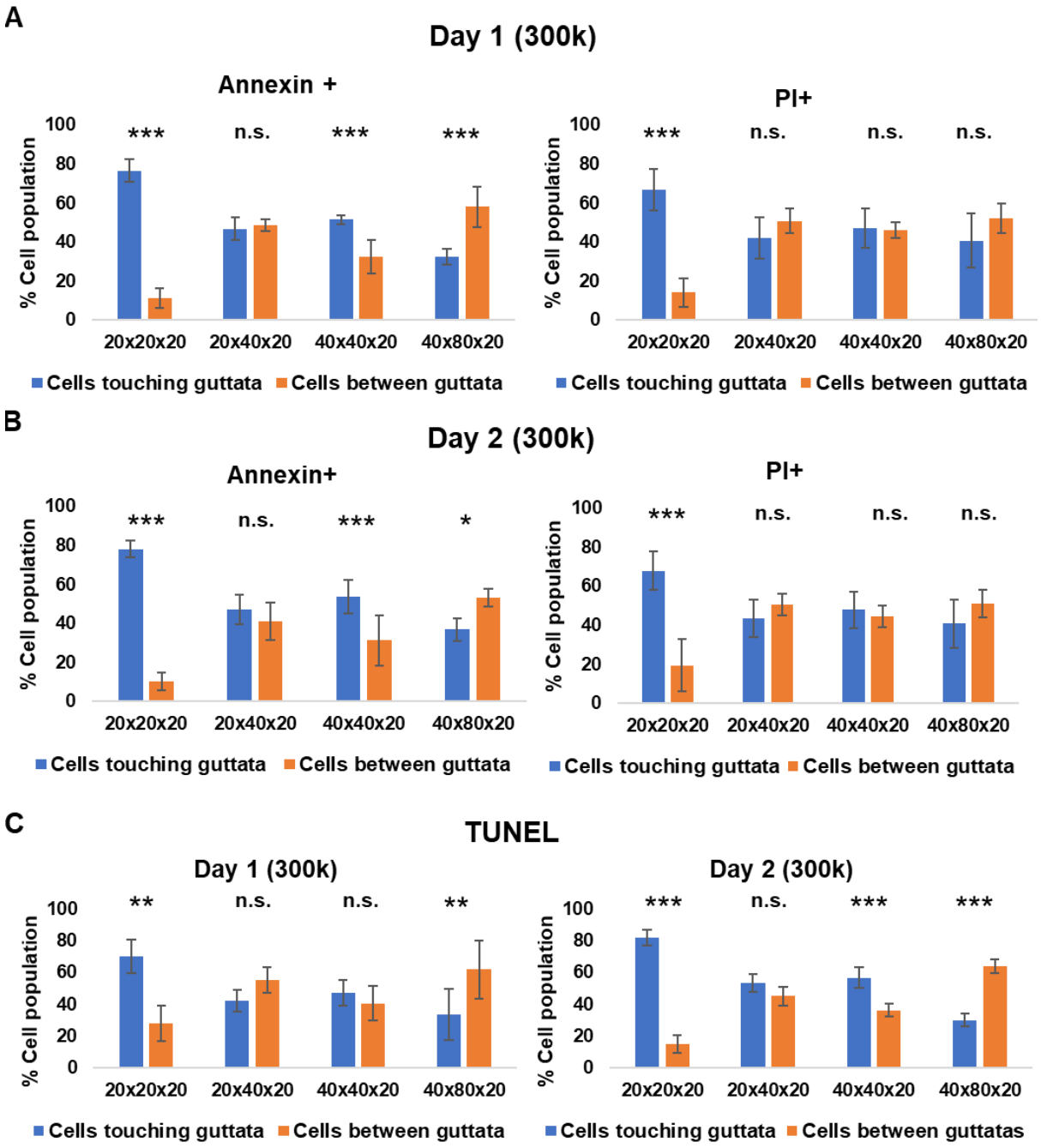

Figure 10: Apoptotic cells localize around guttatas

A) Graphs represent annexin V positive and PI positive cell population localization on Day 1 with respect to s-guttatas.

B) Graphs represent annexin V positive and PI positive cell population localization on Day 2 with respect to s-guttatas.

C) Graphs represent TUNEL positive cell population localization on Day 1 and Day 2 with respect to s-guttatas.

localized around guttatas in comparison to 20x20x20 pattern. 20x40x20 patterns showed 42.0%+/-6.7% and 53.4%+/-5.5% TUNEL positive cell population around guttatas; while 47.2%+/-8.2% and 56.6%+/-6.5% TUNEL positive cell population surrounds 40x40x20 guttatas on Day 1 and Day 2, respectively. In comparison to Day 1, Day 2 had higher percentage of TUNEL positive cells surrounding the s-guttatas. However, this trend was not observed on the 40x80x20 patterns. 33.4%+/-16.0% and 30.0%+/-3.9% TUNEL positive cells were located surrounding s-guttatas on Day 1 and Day 2, respectively. In summary, majority of the apoptotic cells on the 20x20x20, 20x40x20, and 40x40x20 patterns were in proximity to the s-guttata surface. Among them, 20x20x20 patterns had the highest percentage of apoptotic cells adjacent to s-guttatas.

3.3.6 Cytoskeletal stress analysis

In the above results, s-guttata structures have been shown to induce apoptosis, and a large portion of these apoptotic cells surround s-guttatas. Actin, an important component of cytoskeleton, can mediate cell apoptosis and can also trigger cell apoptosis.[129] Hence, actin was stained along with pMLC to analyze cell cytoskeleton on s-guttata patterns. The 20x20x40 and 20x20x60 patterns were chosen as the percentage of apoptotic cells in proximity to s-guttata was higher on these patterns. On Day 1, cells on unpattern substrate had more spread out cells with long actin fibers and uniform pMLC present surrounding fibers (Fig 11). However, on both 20x20x40 and 20x20x60 patterns, some cells surrounding s-guttata showed stronger pMLC and actin expression. Meanwhile, the cells present in between s-guttatas were more spread out with relatively uniform pMLC and actin. Similarly, on Day 2, cells on unpattern substrate had uniform pMLC and actin expression. Consistent to Day 1, some cells surrounding s-guttatas had relatively stronger actin and pMLC expression. Cumulatively, the data demonstrated that cells surrounding

the guttata showed stronger pMLC and actin expression, hence, implying that those cells surrounding s-guttatas may exhibit higher cytoskeletal stress and contractility.

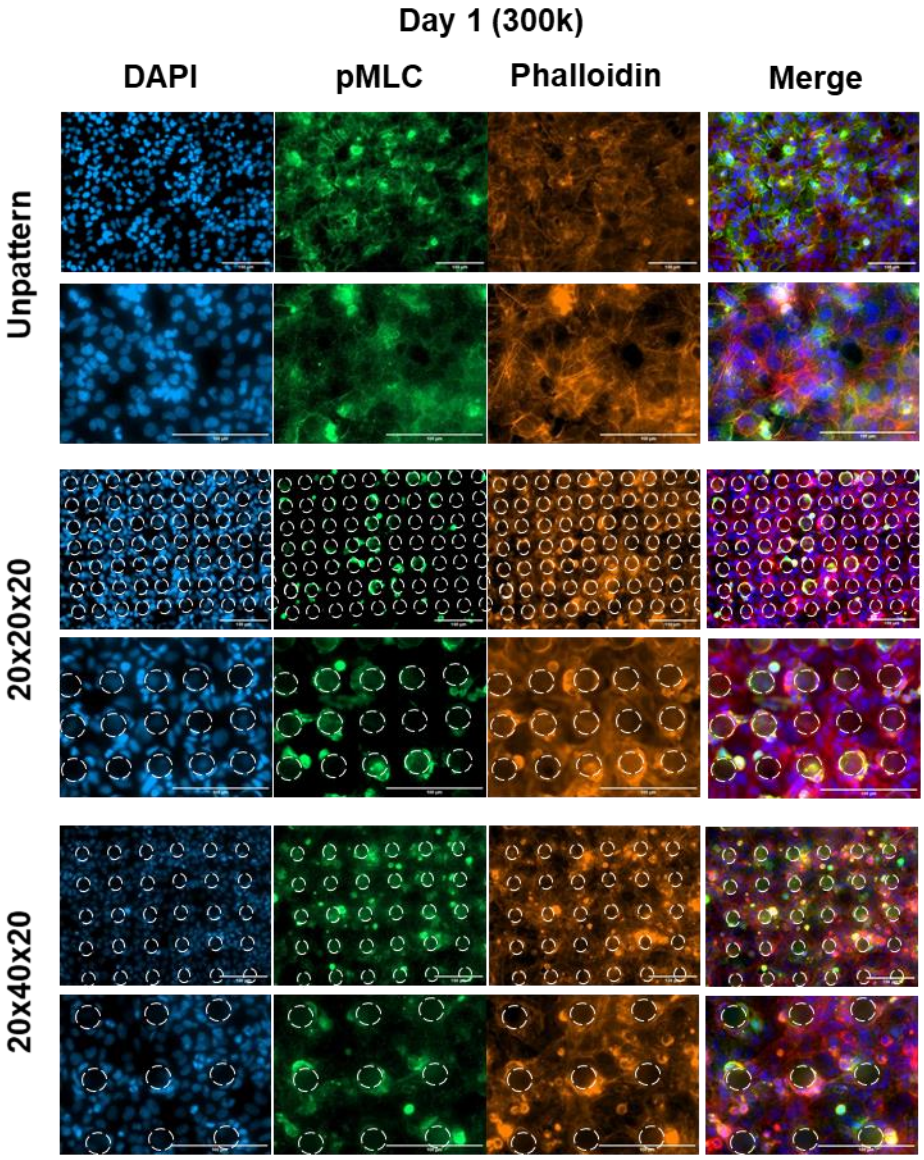

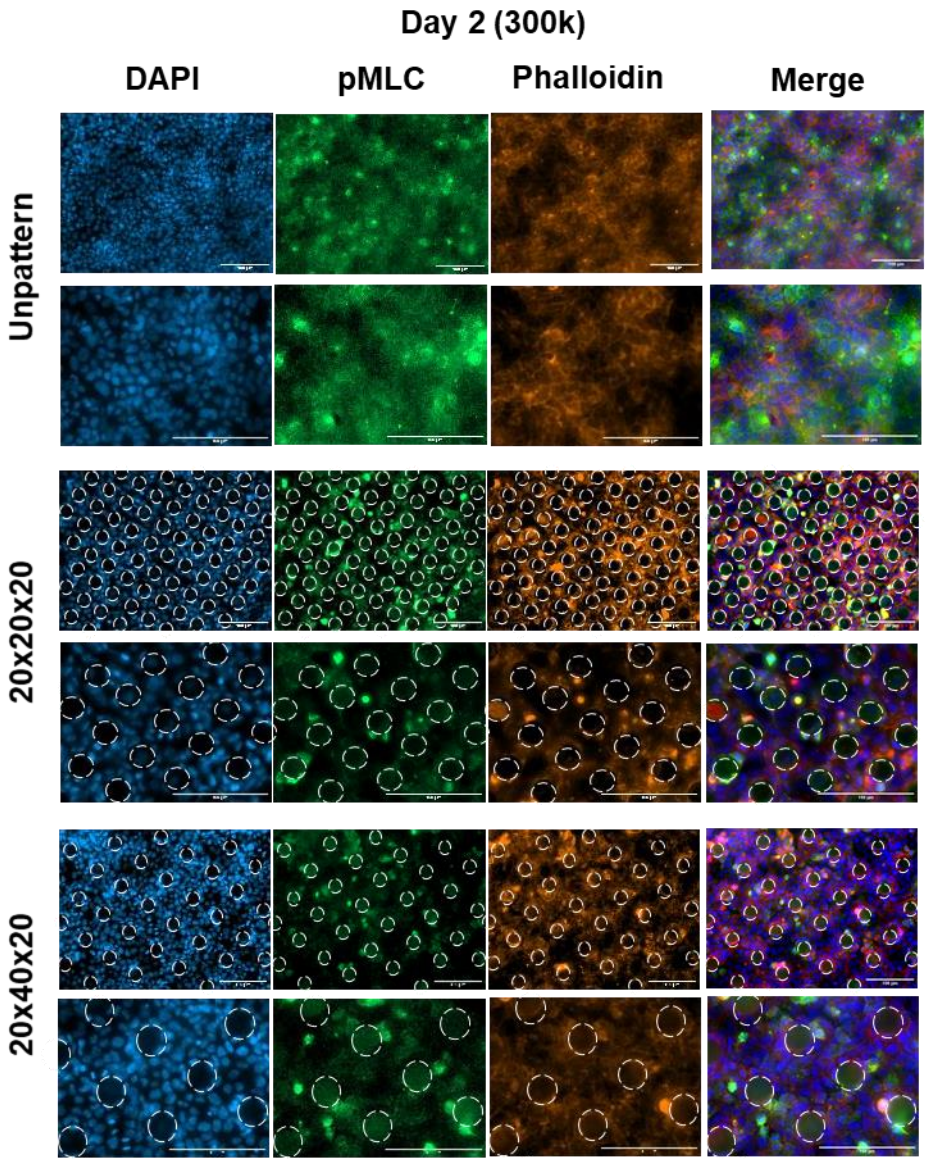

Figure 11: Cells surrounding guttata showed pMLC and phalloidin expression
Representative IF images of cytoskeletal markers (pMLC and phalloidin) staining of corneal endothelial cells seeded on different s-guttata substrates on Day 1 and Day 2. White lines represent guttatas location. Scale bar: 100µm

Surface topographies can induce different cell behaviors such as cell proliferation, cell differentiation, contact guidance, cell migration, cell adhesion, and many more.[95, 130] Previous studies showed that guttatas act as large topographies in the 3D environment, which arises in FED

conditions.[28, 60] These features might impart mechanical cues which further affect corneal endothelial cell loss. In the present chapter, the ability of these large features to induce cell death was uncovered.

3.3.7 Apoptosis and their relationship with guttata

One of the key pathways for corneal endothelial cell loss is cell apoptosis.[105, 106] During FED progression, various conditions are also changed such as oxidative stress, genetic mutations, and the presence of guttatas. Oxidative stress can induce cell apoptosis; and genetic mutations are also correlated with different endothelial cell function related genes.[42, 44, 46] In the development of pharmacotherapy and cell injection therapy, oxidative stress and genetic mutations in diseased cells are partially subsided either by cell proliferative drugs or transplantation of healthy corneal endothelial cells.[84, 127] In these therapies, the guttatas are still intact, and the relevance of these guttatas in the literature has not been yet established. Using *in vitro* FED module, the present work showed that the s-guttatas with a constant height of 20 µm could induce early stage apoptosis irrespective of diameter and spacing. This phenomenon was observed in high and low cell density conditions. It suggests that the irrespective of cell seeding density, these s-guttatas can induce apoptotic stress in the individual cells.

Many studies have investigated corneal endothelial cell apoptosis at different time points.[46, 60, 105, 131] In a recent study, B4G12 cells showed apoptosis induction after a 3h treatment with cumene hydroperoxide, oxidative stress-inducing agent.[131] On native FED DM, HCEnC-21T cell apoptosis was analyzed on the seventh day post-seeding and these cells were apoptotic.[60] Hence, corneal endothelial cell apoptosis induction time can be dependent on the applied treatment or stimulus such as oxidative stress. In this study, we first analyzed B4G12 apoptosis after 24h and 48h after seeding on s-guttata. The apoptotic rates were similar on different time periods in cell

therapy conditions which were between 3-5 folds higher than control. In addition, the percentage of dead cells was lower than apoptotic cells which might indicate that the apoptotic process through this pathway might not be spontaneous. This idea is further strengthened by late stage apoptosis data where the fold rate was 1.5-2 folds higher than the unpattern control in the majority of the s-guttatas on both days. However, the s-guttata with higher spacing and diameter had a relatively high probability to complete the apoptotic process. It is likely that s-guttata dimension can induce differential cell behavior and might also induce differential gene expression in apoptotic pathways. Preliminary experiments with low seeding cell density suggested that cells on s-guttatas can show apoptotic behavior on the seventh day post-seeding (Fig 12). However, it is yet to be determined the minimum time required for s-guttatas to induce corneal endothelial cell apoptosis.

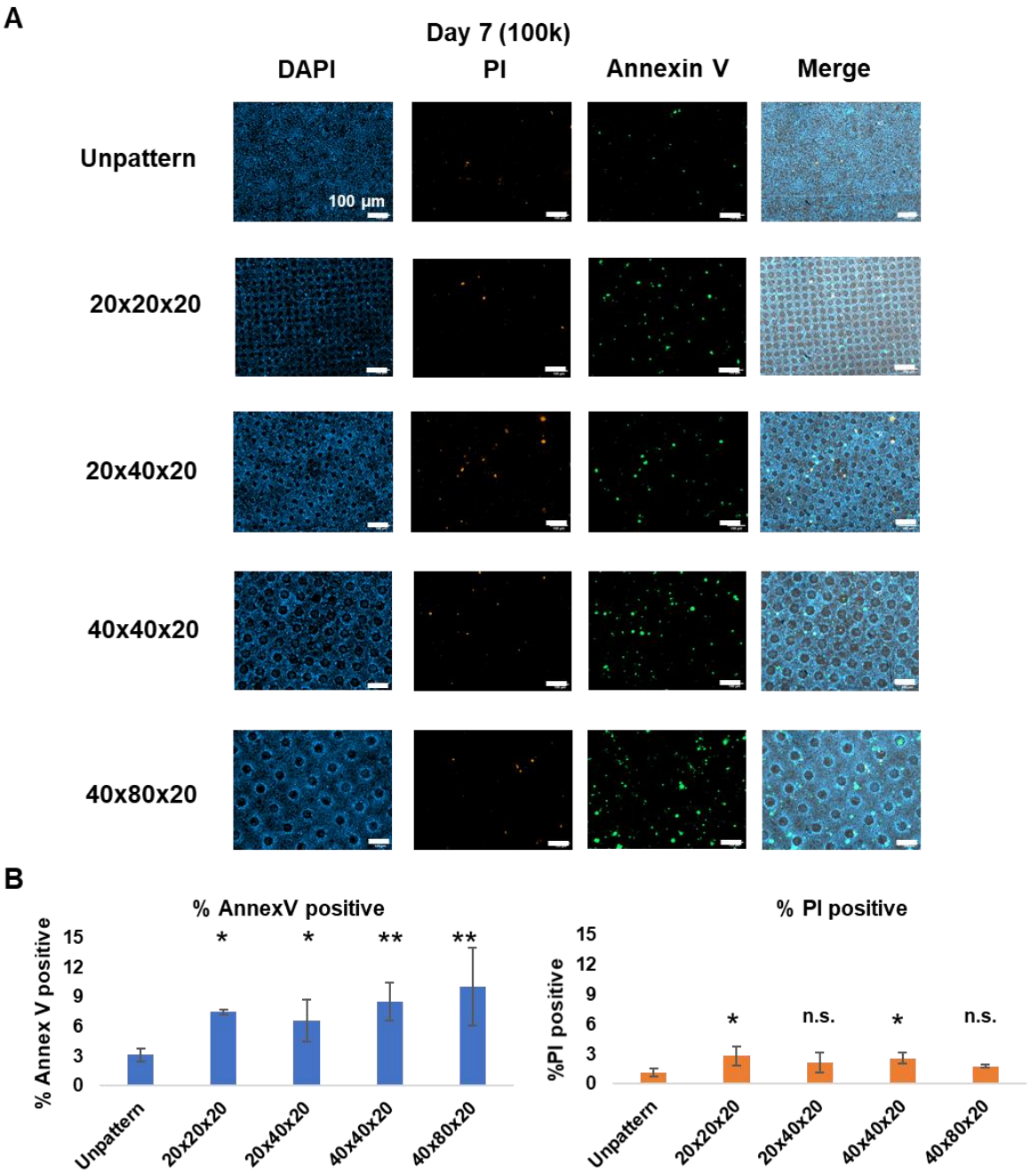

Figure 12: B4G12 cells on s-guttata show higher early stage apoptotic marker expression on Day 7 at lower cell density.

A) Representative IF images of annexin V and PI staining of corneal endothelial cells seeded on different s-guttata substrates. Scale bar: 100µm

*B) Graphs representing annexin V positive and PI positive cell population on different s-guttata patterns. *P < 0.05; **P < 0.01; ***P < 0.001*

3.3.8 Cells experienced cytoskeletal stress around guttatas

Along with apoptosis on s-guttata patterns, the majority of the apoptotic cells in lower spacing were close to s-guttatas in comparison to s-guttatas with higher spacing. There were also apoptotic cells present in between s-guttatas. It is possible that these apoptotic cells might have touched guttatas during their lifetime and these guttatas might have imparted apoptotic cues.

Some cells surrounding guttatas exhibited a relatively stronger pMLC and actin expression. During apoptosis, actin reorganizes and pMLC phosphorylation increases.[111, 115] The higher pMLC expression in cells surrounding s-guttatas suggests that these cells might be going through apoptosis.[116]

3.3.9 Synthetic guttata model follows native FED DM conditions

Cells on s-guttatas with high density, increasing height or large diameter obstructed the complete monolayer formation.[28] Similarly, cells seeded on native FED DM were not able to form a complete monolayer on large diameter in advanced FED DMs.[60] These cells expressed epithelial to mesenchymal transition (EMT) and oxidative stress related genes as well showed apoptosis related damage. FED DM comprises molecules associated with inflammation, aging, and oxidative stress.[26] In addition, FED DM has also varied mechanical properties such as stiffness.[103] It is difficult to distinguish the relevance of the guttata among other confounding factors. Through the s-guttata model, the relevance of s-guttata in cell apoptosis clearly indicated that the removal of guttatas will help to decrease apoptosis and will also help to increase therapy efficiency. Cumulatively, it suggests that the s-guttata model might be an important base for future FED related studies.

3.4 Conclusion

Cells on s-guttata model showed sign of cell apoptosis at high and low cell density conditions. There was similar early stage apoptosis induction among all s-guttata sizes. However, the rate of completing the apoptotic cycle might differ based on s-guttata size. S-Guttatas with larger diameter and higher spacing induced a higher rate of cell death. In addition, apoptotic cells were located close to s-guttatas and prominently highest in 20x20x20 patterns. Cells adjacent to s-guttatas also showed higher cytoskeletal stress. The results indicate that native guttatas alone could interfere with cell therapy by inducing apoptosis in healthy cells. The presence of these guttatas will hamper the efficiency of these therapies and the removal of these guttatas might improve their success rate.

4. Combinatorial effects of substrate stiffness and topography on corneal endothelial cells

4.1 Introduction

Substrate stiffness impacts cell behavior such as adhesion, proliferation, migration, and can also mediate cell apoptosis.[97, 132] In the cornea, stiffness affects multiple cellular functions including epithelial cell adhesion and proliferation, limbus cell differentiation, and corneal endothelial cell proliferation.[104, 133, 134] During disease or injury, extracellular matrix stiffness can be affected leading to change in corneal cell behavior.[133, 135] In FED, Xia et al. observed a decrease in DM stiffness around the guttata region.[103] However, the DM stiffness reported by various groups ranges from 50 kPa-2.6 MPa due to variation in measurement methods. Hence, the appropriate measurement of native tissue stiffness is quite important for rigidity studies.

In the native environment, cells are exposed to various biomechanical and biochemical cues from ECM.[136] In different systems, cumulative effect of substrate topography and stiffness has been reported to regulate stem cell differentiation.[137, 138] During FED native environment, endothelial cells experience dynamic biomechanical and biochemical changes in DM such as guttata formation, stiffness modifications, deposited oxidative stress molecules, and excessive or new matrix ligands representation.[14, 26, 56, 60, 103] These cumulative insults lead to endothelial cell loss and changes in gene expression.[60] The role of these parameters on corneal endothelial cells is either studied individually or their impact is still largely unknown. It has yet to be understood how these factors affect the corneal endothelial cell in the presence of each other. To overcome these challenges, the native DM stiffness in an appropriate environment was measured. A s-guttata system fabricated with gelatin methacrylate (GelMA) can be potentially used to manipulate stiffness. GelMA, synthesized using methacrylate and gelatin, is a biocompatible material and used for various tissue engineering purposes.[139] Furthermore, GelMA can be modulated to obtain a wide range of young's modulus and an ideal candidate for stiffness measurement studies.[89, 139] GelMA

Young's compression modulus can range from 5.8 kPa- 56.7 kPa (10-30% GelMA (w/v) solution) and GelMA+ (sequential hybrid crosslinked form of GelMA) can have Young's compression modulus ranging from 28.8 kPa -233.3 kPa (10-30% GelMA+ (w/v) solution).[89] In this chapter, a preliminary work was performed to demonstrate the feasibility of fabricating s-guttata system with 30% GelMA+.

4.2 Materials and methods

4.2.1 Descemet membrane stiffness measurement

Dr Yam (Singapore Eye Research Center, Singapore, currently in University of Pittsburgh) and Dr Peh (Singapore Eye Research Center, Singapore) dissected DM from human corneas of a 26-year-old male donor. DM membranes were isolated from cornea, decellularized and stored in Optisol-GS (Bausch & Lomb, Bridgewater, NJ, USA) solution at 4ºC using a similar procedure published in Yam et al.[140]. Membrane stiffness were measured through bending test using MicroTester (CellScale, Waterloo) in aqueous conditions at 37ºC using the steps described in the user manual.[141] Briefly, samples were mounted in between two C-shape platforms (made from polylactic acid using a 3D printer, gap = 1.5mm) which were secured by tying up with elastic rubber bands. Furthermore, the load used for measurement was 0 – 57 µN (circular tungsten microbeam diameter = 0.1524 mm).[141] Analysis was done using Microtester software to generate resolved force and displacement readings. Resolved force is calculated through circular tungsten microbeam deflection using the below mentioned equations (available on CellScale MicroTester user manual).[141] In addition, film thickness was measured with different refractive indices (1, 1.35. 1.4; cornea's refractive index lies between 1.35-1.4 [142]) using a 3D laser confocal microscope (LEXT OLS5000, Olympus). Later, these measurements were further analyzed to generate stress

vs strain curves to calculate Young's modulus using the calculations mentioned in compression testing of soft materials module (available on Cellscale website).[143]

$$Deflection = \frac{Force\ x\ Beam\ length^3}{3\ x\ Beam\ Modulus\ x\ Beam\ Area\ Moment\ of\ Inertia}$$

where

$$Beam\ Area\ Moment\ of\ Inertia\ (round) = \frac{\pi\ x\ Radius^4}{4}$$

$$Beam\ Area\ Moment\ of\ Inertia\ (rectangular) = \frac{Width\ x\ Height^3}{12}$$

4.2.2 GelMA+ synthesis and fabrication

Gelatin methacrylate (GelMA) was synthesized using the published protocol.[89] Briefly, 10% w/v gelatin (Type A, Sigma Aldrich) was dissolved in 1x PBS at 50ºC until fully dissolved. 10% methacrylic anhydride (Sigma Aldrich) was added to the solution in a dropwise manner at 50ºC. After complete addition, reaction continued for another 1h. Deionized (DI) water (40ºC) was added in the reaction and left for 5 mins for complete mixing. The reaction mixture was poured in 50ml centrifuge tubes and centrifuged for 5 mins at 5000rpm at RT. Supernatant was filled in 12-14kDa dialysis tubes (Sigma Aldrich) and left in DI water for 5 days at 37°C. Water was changed every day. After 5 days, GelMA solution was poured in 50ml centrifuge tubes and stored at -80ºC for 1 day. Subsequently, this solution was lyophilized and GelMA foam was obtained and stored at -80ºC. Degree of methacrylation was measured using TNBSA assay.

To make GelMA+ hydrogels, GelMA foam was dissolved in 1x PBS containing 0.5% w/v Irgacure 2959 (BASF) at 50°C. Patterned and unpatterened polyethylene terephthalate (PET)

(Goodfellow) molds were prepared using PDMS master molds through embossing.[89] PET molds were adhered to the glass slide and PDMS spacers (thickness 500 µm) were set up on the sides of PET mold. The setup was closed by another glass slide on the top of the spacers and tape. GelMA polymer solution was pipetted on the top of PET mold and between the glass slides. After pouring the polymer solution, the setup was incubated for 1h at 4°C. Later, the solution was crosslinked by using UV irradiation (360-480 nm) at an intensity of 32 mW/cm2 (UVACUBE 100, Honle) for 60s. Crosslinked GelMA+ hydrogels were detached from the PET mold and incubated in 1x PBS at RT.

4.2.3 Cell Culture and cell seeding

B4G12 cell culture was done as mentioned in Chapter 3. For cell culture purposes, GelMA+ hydrogels were washed 3 times using autoclaved PBS and sterilized in UV for 1h. Cells were seeded on the top of hydrogels at the density 300,000/cm^2 and cultured for 48h.

4.2.4 Cytoskeletal staining

Cytoskeletal procedure and analysis were done as mentioned in Chapter 3.

4.2.5 Statistics

Data presented in this chapter were obtained as proof of concept preliminary studies. Number of biological and technical replicas will be indicated for each set of data.

4.3 Results and Discussion

4.3.1 Peripheral and transition zone Descemet membrane stiffness

On basis of location, DM can be categorized in to three parts: central, peripheral, and transition zone (Fig 13).[140] Peripheral and transition zone DM stiffness was measured at different refractive indices. Peripheral DM stiffness was found to be 205 +/-5 kPa (n=1) and transition zone

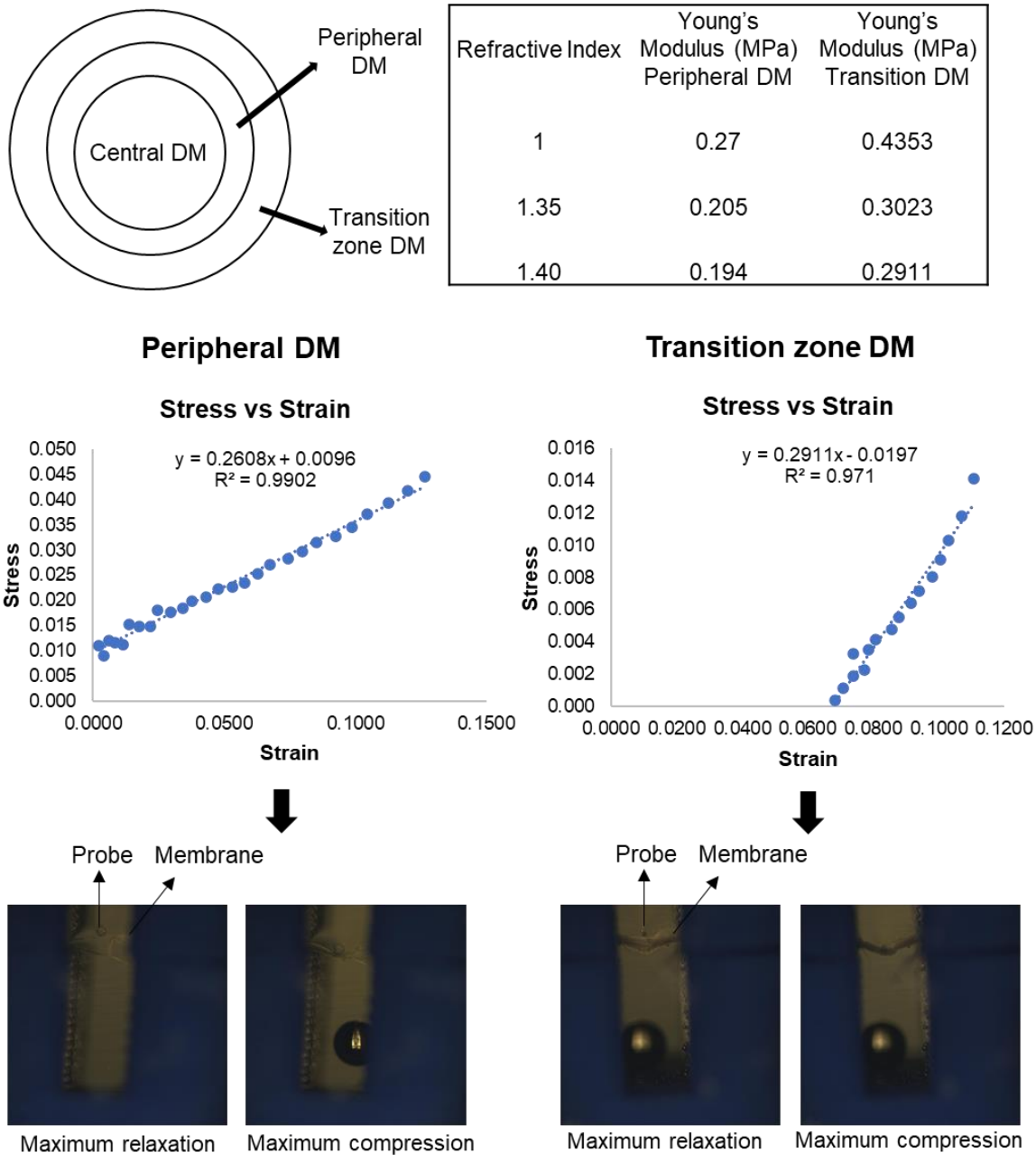

Figure 13: Transitional DM are stiffer than peripheral DM
Stiffness measurements at different refractive index along with their stress and strain curves. Representative images of DM stiffness measurements.

stiffness was 302 +/-6 kPa (n=1) at corneal refractive index (1.35-1.4) (Figure 13). In addition,

the bend in both membranes during the test and stress-strain curves were linear and had a high R-

square value suggesting that the measurements were successful. In summary, hydrated DM stiffness was measured to be in between 200-300 kPa.

4.3.2 Cells cytoskeletal analysis on 30% GelMA+ consisting 20µm guttatas

To analyze the cytoskeletal tension, patterned (20x20x40) and unpatterned hydrogels were fabricated with 30% GelMA+ as the stiffness would be in between 200-300 kPa.[89] Cells formed a monolayer on unpattern substrate, while cells were present in between s-guttatas on patterned substrate (n=1, Fig 14). Unfortunately, the GelMA+ samples showed high autofluorescence with wavelength in the green and red regions. From the preliminary data, apart from few cells, pMLC and actin expression could not be clearly observed in cells on GelMA+ guttata, which was observed in cells on TCPS. Furthermore, the high autofluorescence will need to be resolved and can be mitigated by further optimizing the staining protocol. In addition, for optimum stiffness impact evaluation, cells can be seeded on GelMA+ samples with different rigidities to evaluate stiffness impact, avoiding influence from different surface chemistry when using different materials such as TCPS and GelMA+. This step will help to resolve the issues aroused by using different materials such as surface chemistry and protein adsorption.

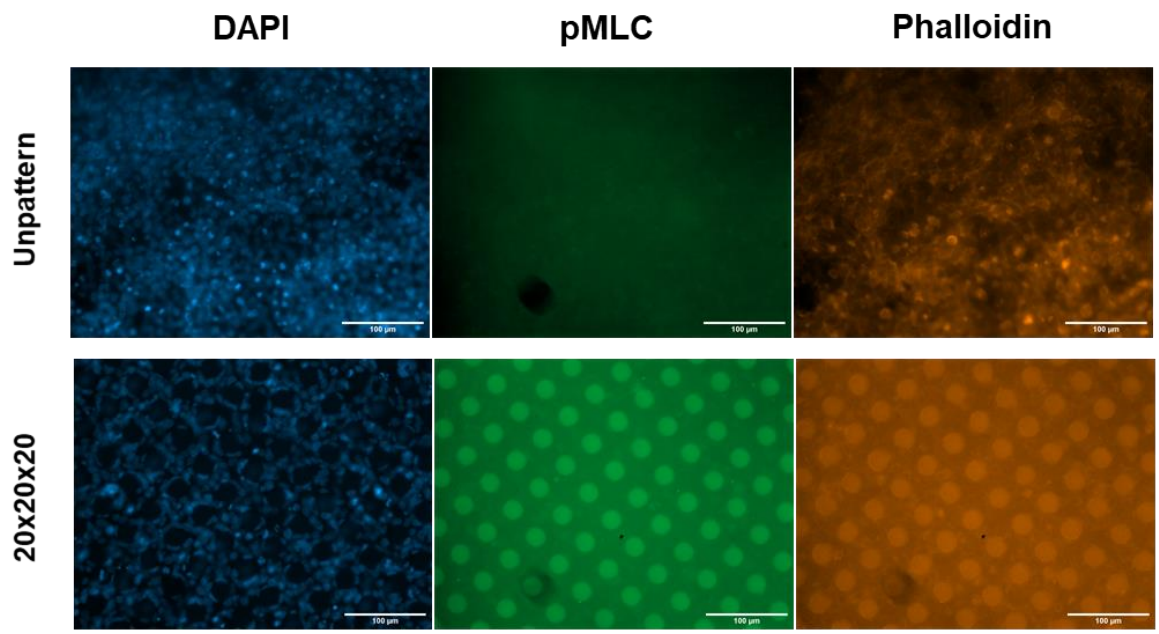

Figure 14: Pattern and unpattern substrate exhibit normal cytoskeletal staining
Representative IF images of cytoskeletal markers (pMLC and phalloidin) staining of CECs seeded on unpattern and 20x20x40 on Day 2. n=1, Scale bar: 100µm

4.4 Conclusion

Previous studies have reported DM stiffness in a wide variety of ranges. Xia et al. reported DM with Young's modulus of 2 MPa through nanoindentation.[103] In contrast, Last et al. reported Young's modulus of 50 kPa using a similar approach.[144] The current preliminary study observed DM stiffness in the range of 200-300 kPa through a 3-point bend test using MicroTester in the physiological conditions. *In vivo*, tissue stiffness can lie in the range of 11 Pa - 20 GPa.[145] Soft tissues such as muscle, skin, and thyroid exhibit stiffness from 1 kPa to 850 kPa. Meanwhile, tissues such as bone, cartilage, and ligament possess stiffness from 5 MPa to 20 GPa. The cornea is a relatively softer tissue than bone or cartilage; it might be possible that cornea stiffness lies in the range of kPa. DM stiffness observed in these studies are also closely related to the readings reported by Last et al.[144] However, further experimentation using different instruments are required to verify the reported readings in this study.

Cumulative effect of stiffness and surface topographies can differentially impact the cell behavior.[137, 138] Synthetic guttatas on TCPS (Young Modulus of 3GPa [146]) are non-flexible and possess a rigid structure. It is likely that cells will sense a higher substrate rigidity and exhibited higher cytoskeletal stress around s-guttatas. Meanwhile, cells were seeded on 30% GelMA+ (Young modulus around 233 kPa [89]). Unfortunately, due to autofluorescence, pMLC and actin expression could not be clearly concluded and require further experimentation. TCPS and GelMA+ are different substrates with different material chemistry such as ligand presentation, ligand density, and protein adsorption.[147, 148] In the future, it would be helpful by using a single type of material to keep its surface chemistry constant. In summary, preliminary studies suggested that DM stiffness was 200-300 kPa which was significantly lower than reported by some studies.

5. Conclusions and Future work

5.1 Conclusions

In this thesis, the role of guttata in cell apoptosis was analyzed. Immortalized human corneal endothelial cells B4G12 were annexin V positive when seeded on s-guttata model at high and low cell density conditions. The percentage of annexin V positive population was similar among all s-guttata sizes. Furthermore, we also observed similar percentage of annexin V positive populations on Day 1 and Day 2 at high and low cell density conditions. TUNEL analysis showed a relative higher percentage of TUNEL positive cell population on s-guttatas, while the highest percentage of TUNEL positive cells were observed on s-guttatas with larger diameter and higher spacing. Upon cell location analysis, both annexin V and TUNEL positive population were located close to s-guttatas. The highest number of positive cell population localized around guttatas was present in 20x20x20 patterns. These studies suggested that guttata environment might have the potential to induce cell apoptosis. Furthermore, cells surrounding guttata also exhibited higher cytoskeletal stress.

Along with the impact of guttatas on cell apoptosis and cell cytoskeleton, preliminary studies were performed to analyze the impact of stiffness. In these studies, peripheral DM stiffness was found to be 205 +/-5 kPa (n=1) and transition zone stiffness was 302 +/-6 kPa (n=1). Furthermore, guttatas were fabricated on 30% GelMA+ which has a Young's modulus around 233 kPa. We performed cytoskeletal staining using this system; however, due to technical issues, we were not able to conclude properly. This part was mostly done as a proof of concept, but future work will be required.

5.2 Future work and recommendations

5.2.1 Synthetic *in vitro* model along with native FED DM for cell apoptosis studies

Native FED DM can induce cell apoptosis in healthy corneal endothelial cells.[60] In an *in vitro* model developed in our research lab, s-guttatas disrupted cell migration and cell monolayer formation.[28] This thesis studies here reported that s-guttatas with 20µm height could induce cell apoptosis at an average rate of 8.2%. Furthermore, it could also lead to cell death. During cell injection therapy, cells are directly seeded on the DM surface.[61] Hence, in the future, the impact of native guttatas on cells can be assessed by scraping the guttata structures from FED DM. This step will likely enhance cell survival and monolayer formation, and it will also help to further identify the role of native guttatas in FED disease.

For current studies, B4G12 cells were used for preliminary studies as they have consistent cell behavior, robust cell source and proliferation. B4G12 cells are proliferative, while primary cells have limited proliferative behavior.[28] Due to their non-proliferative behavior, primary cells would provide a closer view of the native FED condition and might sense the enhanced effect of guttatas in apoptotic as well as depleting monolayer conditions.

5.2.1.1 FED early stage guttata dimensions

We also observed that s-guttata dimensions had a similar induction rate for cell apoptosis. However, the cell death rate was lower than cell apoptosis induction, and it varied across guttata dimensions with the highest in the guttatas with larger spacing and diameter. In addition, s-guttatas with dimensions representing late-stage FED also had a significant effect on monolayer formation where cells were unable to form a monolayer.[28] During the early stage, guttatas dimensions (diameter, height, and density) are smaller; guttatas become larger and higher density structures during disease progression. Guttatas used in current studies majorly represents the late FED stages

i.e. 20 µm height due to the limitation of the proliferative B4G12. To further identify the role of guttata dimensions in early stage FED, it would be interesting to study the cell apoptosis on s-guttatas representing early stages such as 5 µm and 10 µm height guttatas using primary human corneal endothelial cells.

5.2.1.2 Temporal behavior of guttata for cell apoptosis analysis

In this thesis, cell apoptosis induction and cell death were studied for post 24h and 48h after cell introduced to the s-guttatas. These studies can be utilized to understand the initial impact of s-guttatas on cells seeded on the FED DM surface. However, the results obtained from annexin V and TUNEL data in this duration might not completely cover the extent of guttata's influence in cell apoptosis. FED is a degenerative disorder and it takes a long time to reduce the percentage of the non-proliferative corneal endothelial cell population.[105] Hence, a prolonged study such as 7 days to 30 days will help to further decipher the impact of s-guttata dimensions on the cell death rate. In addition, FED guttata formation is a dynamic process. These guttatas develop from smaller and less confluent structures to larger and highly confluent ones. Corneal endothelial cells also experience this dynamic behavior and might perceive different mechanical cues based on guttata dimensions. To mimic this dynamic behavior, cells can be transferred after culturing on early stage guttatas to late stage guttatas and analyzed for cell apoptosis. It will help to unravel the effects of dynamic cues perceived by corneal endothelial cells on their apoptotic behavior.

5.2.2 Cell membrane tension studies

Through these studies, we observed cytoskeletal changes in the cells surrounding guttatas. In addition, guttatas might modulate changes in cell membrane tension during wrapping or stretching around guttatas. Osmotic pressure is generally used to modulate cell membrane tension; however, the effect of osmotic pressure on cell membrane tension is still debatable.[149] In our

preliminary experiment, we observed comparatively increased annexin V positive population in B4G12 upon changing osmotic pressure using D-sorbitol (hypertonic) and water (hypotonic) (Fig 15). In the future, these studies can be expanded to analyze the effect of osmotic pressure changes on cells seeded on guttatas. Along with osmotic pressure, cell membrane tension can also be quantified using FliptR technology (Spirochrome, USA) and FLIM imaging system (Olympus).[150] These studies will help us to evaluate changes in cell membrane tension due to guttatas as well as the impact of cell membrane tension changes on cell apoptosis.

5.2.2.1 ROCK signaling studies

ROCK inhibitor enhances corneal endothelial proliferation, adhesion, and migration.[76, 77, 124] The effect of ROCK inhibitor is yet to be understood in FED guttatas. The application of ROCK inhibitor in the s-guttatta model will help to determine the rescue effect of this treatment in cell apoptosis. In addition, this inhibitor can also be applied in native FED DM. These studies will help to identify the potential of ROCK treatment in rescuing cells from FED phenotype as well as if ROCK treatment can successfully overcome the guttatas toxic behavior. Furthermore, ROCK proteins can act in caspase dependent or independent pathways.[124, 151] To determine the changes in caspase expression levels, B4G12 cells seeded on guttatas were stained for caspase proteins using a caspase cocktail kit. Visually, the expression levels seemed to be similar across different conditions (guttatas and unpattern TCPS substrate). However, these experiments need to be repeated, and q-PCR can be done to analyze relative expression levels. However, it is possible from this preliminary experiment that ROCK proteins might be acting in a caspase independent manner in corneal endothelial cells.

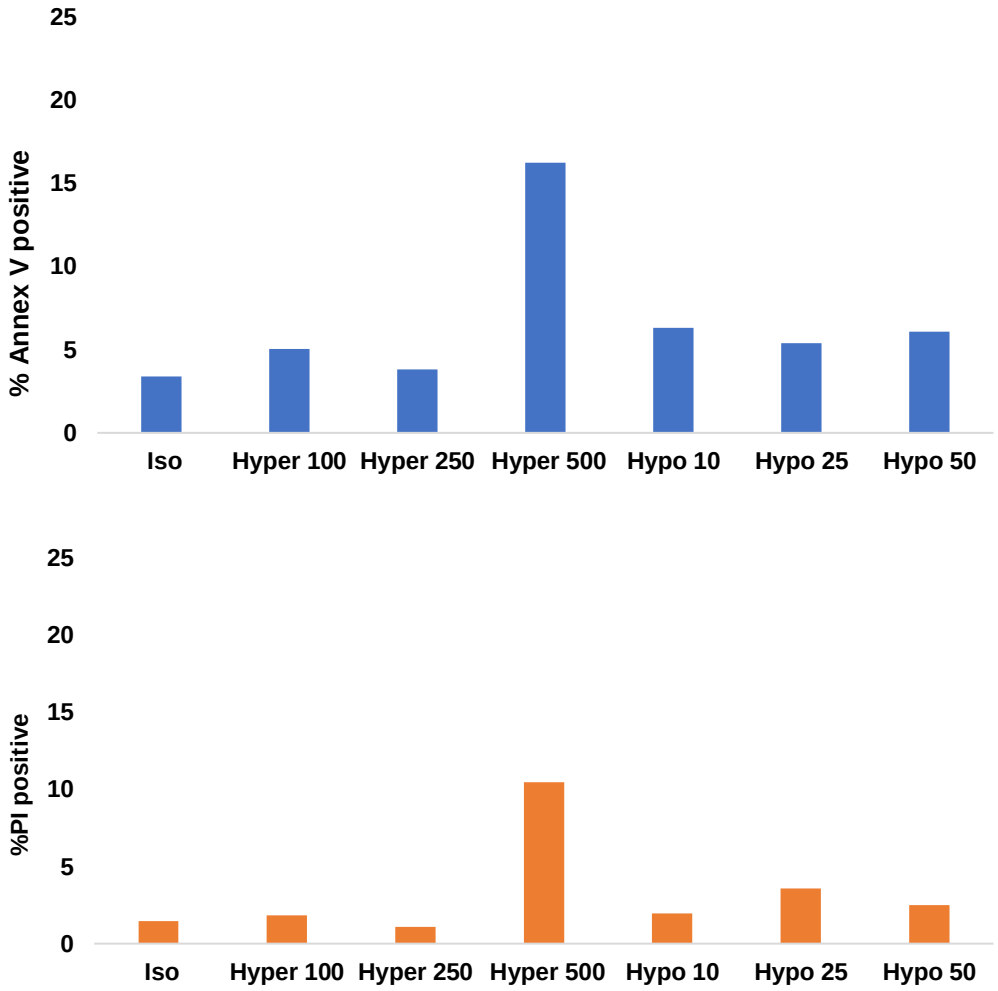

Figure 15: Annexin V and PI percentage positive B4G12 cells graphs 24h after seeding at a cell density 300k on an unpatterned substrate.
Iso – Normal media, Hyper 100 – 100mM D-sorbitol in media, Hyper 250 – 250mM D-sorbitol in media, Hyper 500 – 500mM D-sorbitol in media, Hypo 10 – Media diluted with additional 10% dI water, Hypo 25 – Media diluted with additional 25% dI water, Hypo 50 – Media diluted with additional 50% dI water. N=1

5.2.3 FED *in vitro* model development using *in vivo* stiffness measurements

Peripheral DM and Transition zone DM had a stiffness of 305 kPa and 302 kPa, respectively. These measurements lie in the reported wide range of DM stiffness.[133] However, the reported measurements are still yet to be verified. To overcome this, DM stiffness can be measured through AFM and Microtester to verify the measurement repeatability in aqueous conditions. The

stiffness measurement of FED DM guttatas along with varied guttata dimensions will provide the appropriate environment for further development of the in vitro FED model. It will further help to understand the combinatorial biomechanical studies by assessing their impact on cell apoptosis and cell death.

5.2.3.1 GelMA+ stiffness modulation along with guttatas

Influenced by the auto-fluorescence of the GelMA+ sample, we could not conclude the effect of 30% GelMA+ on cell cytoskeleton. However, due to the lower stiffness of 30% GelMA+ than TCPS substrate, low cytoskeletal tension was expected as compared to TCPS substrates. Furthermore, TCPS and GelMA have different surface chemistry and observed stiffness effects might also be affected by material's surface properties. In future, it would be relevant to use GelMA+ or GelMA and varies its stiffness by changing GelMA+ or GelMA concentration. Furthermore, it will also be interesting to observe the combinatorial effect of stiffness and topography by varying the GelMA+ stiffness of the material along with the presence of guttatas.

6. Additional contributions to other projects:

1. Isotropic topographies for mESC expansion - Potential authors: Sarah Chan, Rizwan Muhammad, Deepak Jain, and Evelyn Yim
2. Influence of isotropic and anisotropic topographies on human skeletal muscle - Potential authors: Sabrina Mattiasi, Sadegh Davoudi, Deepak Jain, Penny Gilbert and Evelyn Yim

7. Publications published from contributions to other projects:

1. Jain D*, Mattiassi S*, Goh EL, Yim EKF. Extracellular matrix and biomimetic engineering microenvironment for neuronal differentiation. *Neural Regen Res*. **2020**;15(4):573-585.

2. Sharvari Sathe*, Deepak Jain*, Cheng-Gee Koh and Evelyn K.F. Yim. Effects of POPX2 and topographical contact guidance on cell morphology and migration. *ACS Biomaterials Science and Engineering* (In review)

   * - Authors contributed equally

8. References:

1. DelMonte, D. W.; Kim, T., Anatomy and physiology of the cornea. *Journal of Cataract & Refractive Surgery* **2011,** *37* (3).
2. Eghrari, A. O.; Riazuddin, S. A.; Gottsch, J. D., Chapter Two - Overview of the Cornea: Structure, Function, and Development. In *Progress in Molecular Biology and Translational Science*, Hejtmancik, J. F.; Nickerson, J. M., Eds. Academic Press: 2015; Vol. 134, pp 7-23.
3. Sridhar, M., Anatomy of cornea and ocular surface. **2018,** *66* (2), 190-194.
4. Mochizuki, H.; Fukui M Fau - Hatou, S.; Hatou S Fau - Yamada, M.; Yamada M Fau - Tsubota, K.; Tsubota, K., Evaluation of ocular surface glycocalyx using lectin-conjugated fluorescein. *Clinical Ophthalmology* **2010,** *4* (1177-5483 (Electronic)).
5. Li, W.; Hayashida, Y.; Chen, Y.-T.; Tseng, S. C. G., Niche regulation of corneal epithelial stem cells at the limbus. *Cell Research* **2007,** *17* (1), 26-36.
6. Tuori, A.; Uusitalo, H.; Burgeson, R. E.; Terttunen, J.; Virtanen, I., The Immunohistochemical Composition of the Human Corneal Basement Membrane. *Cornea* **1996,** *15* (3).
7. Torricelli, A. A. M.; Singh, V.; Santhiago, M. R.; Wilson, S. E., The Corneal Epithelial Basement Membrane: Structure, Function, and Disease. *Investigative Ophthalmology & Visual Science* **2013,** *54* (9), 6390-6400.
8. Pal-Ghosh, S.; Pajoohesh-Ganji, A.; Tadvalkar, G.; Stepp, M. A., Removal of the basement membrane enhances corneal wound healing. *Experimental eye research* **2011,** *93* (6), 927-936.
9. Wilson, S. E.; Hong, J.-W., Bowman's Layer Structure and Function: Critical or Dispensable to Corneal Function? A Hypothesis. *Cornea* **2000,** *19* (4).
10. Boote, C.; Dennis, S.; Newton, R. H.; Puri, H.; Meek, K. M., Collagen Fibrils Appear More Closely Packed in the Prepupillary Cornea: Optical and Biomechanical Implications. *Investigative Ophthalmology & Visual Science* **2003,** *44* (7), 2941-2948.
11. Hamrah, P.; Dana, M., Corneal Antigen-Presenting Cells. *Chemical Immunology and Allergy* **2007,** *92*, 58-70.
12. Murphy, C.; Alvarado, J.; Juster, R., Prenatal and postnatal growth of the human Descemet's membrane. *Investigative Ophthalmology & Visual Science* **1984,** *25* (12), 1402-1415.
13. Sawada, H.; Konomi, H.; Hirosawa, K., Characterization of the collagen in the hexagonal lattice of Descemet's membrane: its relation to type VIII collagen. *Journal of Cell Biology* **1990,** *110* (1), 219-227.
14. Ali, M.; Raghunathan, V.; Li, J. Y.; Murphy, C. J.; Thomasy, S. M., Biomechanical relationships between the corneal endothelium and Descemet's membrane. *Experimental eye research* **2016,** *152*, 57-70.
15. Tuft, S. J.; Coster, D. J., The corneal endothelium. *Eye* **1990,** *4* (3), 389-424.
16. Joyce, N. C.; Navon, S. E.; Roy, S.; Zieske, J. D., Expression of cell cycle-associated proteins in human and rabbit corneal endothelium in situ. *Investigative Ophthalmology & Visual Science* **1996,** *37* (8), 1566-1575.
17. Bourne, W. M., Biology of the corneal endothelium in health and disease. *Eye* **2003,** *17* (8), 912-918.
18. Matsubara M Fau - Tanishima, T.; Tanishima, T., Wound-healing of corneal endothelium in monkey: an autoradiographic study. *Jpn J Ophthalmol.* **1983,** *27* (3), 444-50.
19. Matsuda, M.; Sawa, M.; Edelhauser, H. F.; Bartels, S. P.; Neufeld, A. H.; Kenyon, K. R., Cellular migration and morphology in corneal endothelial wound repair. *Investigative Ophthalmology & Visual Science* **1985,** *26* (4), 443-449.
20. Van den Bogerd, B.; Dhubhghaill, S. N.; Koppen, C.; Tassignon, M.-J.; Zakaria, N., A review of the evidence for in vivo corneal endothelial regeneration. *Survey of Ophthalmology* **2018,** *63* (2), 149-165.

21. Bourne, W. M., Primary Corneal Endotheliopathies. *American Journal of Ophthalmology* **1983,** *95* (6), 852-853.
22. Krachmer, J. H., Posterior polymorphous corneal dystrophy: a disease characterized by epithelial-like endothelial cells which influence management and prognosis. *Trans Am Ophthalmol Soc.* **1985,** *83* (413-75).
23. Patel, S. P.; Parker, M. D., SLC4A11 and the Pathophysiology of Congenital Hereditary Endothelial Dystrophy. *Biomed Res Int.* **2015,** (2314-6141 (Electronic)).
24. Feizi, S., Corneal endothelial cell dysfunction: etiologies and management. *Therapeutic Advances in Ophthalmology* **2018,** *10*, 2515841418815802.
25. Vedana, G.; Villarreal, G., Jr.; Jun, A. S., Fuchs endothelial corneal dystrophy: current perspectives. *Clin Ophthalmol.* **2016,** *10* (321-30).
26. Eghrari, A. O.; Riazuddin, S. A.; Gottsch, J. D., Chapter Seven - Fuchs Corneal Dystrophy. In *Progress in Molecular Biology and Translational Science*, Hejtmancik, J. F.; Nickerson, J. M., Eds. Academic Press: 2015; Vol. 134, pp 79-97.
27. Soh, Y. Q.; Kocaba, V.; Pinto, M.; Mehta, J. S., Fuchs endothelial corneal dystrophy and corneal endothelial diseases: East meets West. *Eye* **2019**.
28. Rizwan, M.; Peh, G. S.; Adnan, K.; Naso, S. L.; Mendez, A. R.; Mehta, J. S.; Yim, E. K. F., In Vitro Topographical Model of Fuchs Dystrophy for Evaluation of Corneal Endothelial Cell Monolayer Formation. *Advanced Healthcare Materials* **2016,** *5* (22), 2896-2910.
29. Bourne, W. M.; Johnson, D. H.; Campbell, R. J., The Ultrastructure of Descemet's Membrane: III. Fuchs' Dystrophy. *Archives of Ophthalmology* **1982,** *100* (12), 1952-1955.
30. Wilson, S. E.; Bourne, W. M., Fuchs' dystrophy. *Cornea* **1988,** *7* (1), 2-18.
31. Adamis, A. P.; Filatov, V.; Tripathi, B. J.; Tripathi, R. A. m. C., Fuchs' endothelial dystrophy of the cornea. *Survey of Ophthalmology* **1993,** *38* (2), 149-168.
32. Gain, P.; Jullienne, R.; He, Z.; Aldossary, M.; Acquart, S.; Cognasse, F.; Thuret, G., Global Survey of Corneal Transplantation and Eye Banking. *JAMA Ophthalmology* **2016,** *134* (2), 167-173.
33. Chan, S. W. S.; Yucel, Y.; Gupta, N., New trends in corneal transplants at the University of Toronto. *Canadian Journal of Ophthalmology* **2018,** *53* (6), 580-587.
34. Bigan, G.; Puyraveau, M.; Saleh, M.; Gain, P.; Martinache, I.; Delbosc, B.; Gauthier, A.-S., Corneal transplantation trends in France from 2004 to 2015: A 12-year review. *European Journal of Ophthalmology* **2018,** *28* (5), 535-540.
35. Lorenzetti, D. W. C.; Uotila, M. H.; Parikh, N.; Kaufman, H. E., Central Cornea Guttata: Incidence in the General Population. *American Journal of Ophthalmology* **1967,** *64* (6), 1155-1158.
36. Krachmer, J. H.; Purcell, J. J., Jr.; Young, C. W.; Bucher, K. D., Corneal Endothelial Dystrophy: A Study of 64 Families. *Archives of Ophthalmology* **1978,** *96* (11), 2036-2039.
37. Zoega, G. M.; Fujisawa, A.; Sasaki, H.; Kubota, A.; Sasaki, K.; Kitagawa, K.; Jonasson, F., Prevalence and Risk Factors for Cornea Guttata in the Reykjavik Eye Study. *Ophthalmology* **2006,** *113* (4), 565-569.
38. Eghrari, A. O.; McGlumphy, E. J.; Iliff, B. W.; Wang, J.; Emmert, D.; Riazuddin, S. A.; Katsanis, N.; Gottsch, J. D., Prevalence and Severity of Fuchs Corneal Dystrophy in Tangier Island. *American Journal of Ophthalmology* **2012,** *153* (6), 1067-1072.
39. Louttit, M. D.; Kopplin, L. J.; Igo, R. P., Jr.; Fondran, J. R.; Tagliaferri, A.; Bardenstein, D.; Aldave, A. J.; Croasdale, C. R.; Price, M. O.; Rosenwasser, G. O.; Lass, J. H.; Iyengar, S. K.; for the, F. G. M.-C. S. G., A Multicenter Study to Map Genes for Fuchs Endothelial Corneal Dystrophy: Baseline Characteristics and Heritability. *Cornea* **2012,** *31* (1).
40. Gottsch, J. D.; Sundin, O. H.; Liu, S. H.; Jun, A. S.; Broman, K. W.; Stark, W. J.; Vito, E. C. L.; Narang, A. K.; Thompson, J. M.; Magovern, M., Inheritance of a Novel COL8A2 Mutation Defines a Distinct Early-Onset Subtype of Fuchs Corneal Dystrophy. *Investigative Ophthalmology & Visual Science* **2005,** *46* (6), 1934-1939.
41. Biswas, S.; Munier, F. L.; Yardley, J.; Hart-Holden, N.; Perveen, R.; Cousin, P.; Sutphin, J. E.; Noble, B.; Batterbury, M.; Kielty, C.; Hackett, A.; Bonshek, R.; Ridgway, A.; McLeod, D.;

Sheffield, V. C.; Stone, E. M.; Schorderet, D. F.; Black, G. C. M., Missense mutations in COL8A2, the gene encoding the α2 chain of type VIII collagen, cause two forms of corneal endothelial dystrophy. *Human Molecular Genetics* **2001,** *10* (21), 2415-2423.
42. Zhang, J.; McGhee, C. N. J.; Patel, D. V., The Molecular Basis of Fuchs' Endothelial Corneal Dystrophy. *Molecular Diagnosis & Therapy* **2019,** *23* (1), 97-112.
43. Sarnicola, C.; Farooq, A. V.; Colby, K., Fuchs Endothelial Corneal Dystrophy: Update on Pathogenesis and Future Directions. **2019,** *45* (1), 1-10.
44. Jurkunas, U. V.; Bitar, M. S.; Funaki, T.; Azizi, B., Evidence of Oxidative Stress in the Pathogenesis of Fuchs Endothelial Corneal Dystrophy. *The American Journal of Pathology* **2010,** *177* (5), 2278-2289.
45. Gottsch, J. D.; Bowers, A. L.; Margulies, E. H.; Seitzman, G. D.; Kim, S. W.; Saha, S.; Jun, A. S.; Stark, W. J.; Liu, S. H., Serial Analysis of Gene Expression in the Corneal Endothelium of Fuchs' Dystrophy. *Investigative Ophthalmology & Visual Science* **2003,** *44* (2), 594-599.
46. Azizi, B.; Ziaei, A.; Fuchsluger, T.; Schmedt, T.; Chen, Y.; Jurkunas, U. V., p53-Regulated Increase in Oxidative-Stress–Induced Apoptosis in Fuchs Endothelial Corneal Dystrophy: A Native Tissue Model. *Investigative Ophthalmology & Visual Science* **2011,** *52* (13), 9291-9297.
47. Miyai, T., Fuchs Endothelial Corneal Dystrophy and Mitochondria. *Cornea* **2018,** *37*.
48. Engler, C.; Kelliher, C.; Spitze, A. R.; Speck, C. L.; Eberhart, C. G.; Jun, A. S., Unfolded Protein Response in Fuchs Endothelial Corneal Dystrophy: A Unifying Pathogenic Pathway? *American Journal of Ophthalmology* **2010,** *149* (2), 194-202.e2.
49. Okumura, N.; Kitahara, M.; Okuda, H.; Hashimoto, K.; Ueda, E.; Nakahara, M.; Kinoshita, S.; Young, R. D.; Quantock, A. J.; Tourtas, T.; Schlötzer-Schrehardt, U.; Kruse, F.; Koizumi, N., Sustained Activation of the Unfolded Protein Response Induces Cell Death in Fuchs' Endothelial Corneal Dystrophy. *Investigative Ophthalmology & Visual Science* **2017,** *58* (9), 3697-3707.
50. Alvarez-Garcia, I.; Miska, E. A., MicroRNA functions in animal development and human disease. *Development* **2005,** *132* (21), 4653.
51. Matthaei, M.; Hu, J.; Kallay, L.; Eberhart, C. G.; Cursiefen, C.; Qian, J.; Lackner, E.-M.; Jun, A. S., Endothelial Cell MicroRNA Expression in Human Late-Onset Fuchs' Dystrophy. *Investigative Ophthalmology & Visual Science* **2014,** *55* (1), 216-225.
52. Ueno, M.; Asada, K.; Toda, M.; Hiraga, A.; Montoya, M.; Sotozono, C.; Kinoshita, S.; Hamuro, J., MicroRNA Profiles Qualify Phenotypic Features of Cultured Human Corneal Endothelial Cells. *Investigative Ophthalmology & Visual Science* **2016,** *57* (13), 5509-5517.
53. Okumura, N.; Minamiyama, R.; Ho, L. T. Y.; Kay, E. P.; Kawasaki, S.; Tourtas, T.; Schlötzer-Schrehardt, U.; Kruse, F. E.; Young, R. D.; Quantock, A. J.; Kinoshita, S.; Koizumi, N., Involvement of ZEB1 and Snail1 in excessive production of extracellular matrix in Fuchs endothelial corneal dystrophy. *Laboratory Investigation* **2015,** *95* (11), 1291-1304.
54. Katikireddy, K. R.; White, T. L.; Miyajima, T.; Vasanth, S.; Raoof, D.; Chen, Y.; Price, M. O.; Price, F. W.; Jurkunas, U. V., NQO1 downregulation potentiates menadione-induced endothelial-mesenchymal transition during rosette formation in Fuchs endothelial corneal dystrophy. *Free Radical Biology and Medicine* **2018,** *116*, 19-30.
55. Jackson, A. J.; Robinson, F. O.; Frazer, D. G.; Archer, D. B., Corneal guttata: A comparative clinical and specular micrographic study. *Eye* **1999,** *13* (6), 737-743.
56. Waring, G. O.; Bourne, W. M.; Edelhauser, H. F.; Kenyon, K. R., The Corneal Endothelium: Normal and Pathologic Structure and Function. *Ophthalmology* **1982,** *89* (6), 531-590.
57. Elhalis, H.; Azizi, B.; Jurkunas, U. V., Fuchs Endothelial Corneal Dystrophy. *The Ocular Surface* **2010,** *8* (4), 173-184.
58. Bergmanson, J. P. G.; Sheldon, T. M.; Goosey, J. D., Fuchs' endothelial dystrophy: a fresh look at an aging disease. *Ophthalmic and Physiological Optics* **1999,** *19* (3), 210-222.
59. Jurkunas, U. V.; Bitar, M. S.; Rawe, I.; Harris, D. L.; Colby, K.; Joyce, N. C., Increased Clusterin Expression in Fuchs' Endothelial Dystrophy. *Investigative Ophthalmology & Visual Science* **2008,** *49* (7), 2946-2955.

60. Kocaba, V.; Katikireddy, K. R.; Gipson, I.; Price, M. O.; Price, F. W.; Jurkunas, U. V., Association of the Gutta-Induced Microenvironment With Corneal Endothelial Cell Behavior and Demise in Fuchs Endothelial Corneal Dystrophy. *JAMA Ophthalmology* **2018,** *136* (8), 886-892.
61. Soh, Y. Q.; Peh, G. S. L.; Mehta, J. S., Evolving therapies for Fuchs' endothelial dystrophy. *Regenerative Medicine* **2018,** *13* (1), 97-115.
62. Rahman, I.; Carley, F.; Hillarby, C.; Brahma, A.; Tullo, A. B., Penetrating keratoplasty: indications, outcomes, and complications. *Eye* **2009,** *23* (6), 1288-1294.
63. de la Paz, M. F.; Sibila, G. R.; Montenegro, G.; de Toledo, J. A.; Michael, R.; Barraquer, R.; Barraquer, J., Wedge Resection for High Astigmatism After Penetrating Keratoplasty for Keratoconus: Refractive and Histopathologic Changes. *Cornea* **2010,** *29* (6).
64. Liu, M.; Hong, J. A.-O., Risk Factors for Endothelial Decompensation after Penetrating Keratoplasty and Its Novel Therapeutic Strategies. *J Ophthalmol.* **2018**, 1389486.
65. Böhringer, D.; Böhringer, S.; Poxleitner, K.; Birnbaum, F.; Schwartzkopff, J.; Maier, P.; Sundmacher, R.; Reinhard, T., Long-Term Graft Survival in Penetrating Keratoplasty: The Biexponential Model of Chronic Endothelial Cell Loss Revisited. *Cornea* **2010,** *29* (10).
66. Price, M. O.; Gupta, P.; Lass, J.; Price, F. W., EK (DLEK, DSEK, DMEK): New Frontier in Cornea Surgery. *Annual Review of Vision Science* **2017,** *3* (1), 69-90.
67. Terry, M. A., Deep lamellar endothelial keratoplasty (DLEK): pursuing the ideal goals of endothelial replacement. *Eye* **2003,** *17* (8), 982-988.
68. Melles, G. R. J.; Wijdh, R. H. J.; Nieuwendaal, C. P., A Technique to Excise the Descemet Membrane From a Recipient Cornea (Descemetorhexis). *Cornea* **2004,** *23* (3).
69. Lee, W. B.; Jacobs, D. S.; Musch, D. C.; Kaufman, S. C.; Reinhart, W. J.; Shtein, R. M., Descemet's Stripping Endothelial Keratoplasty: Safety and Outcomes: A Report by the American Academy of Ophthalmology. *Ophthalmology* **2009,** *116* (9), 1818-1830.
70. Melles, G. R. J.; Lander, F.; Rietveld, F. J. R., Transplantation of Descemet's Membrane Carrying Viable Endothelium Through a Small Scleral Incision. *Cornea* **2002,** *21* (4).
71. Melles, G. R. J., Posterior Lamellar Keratoplasty: DLEK to DSEK to DMEK. *Cornea* **2006,** *25* (8).
72. Deng, S. X.; Lee, W. B.; Hammersmith, K. M.; Kuo, A. N.; Li, J. Y.; Shen, J. F.; Weikert, M. P.; Shtein, R. M., Descemet Membrane Endothelial Keratoplasty: Safety and Outcomes: A Report by the American Academy of Ophthalmology. *Ophthalmology* **2018,** *125* (2), 295-310.
73. 2016 EYE BANKING STATISTICAL REPORT. *Eye Bank Association of America* **2016**.
74. Córdoba, A.; Mejía, L. F.; Mannis, M. J.; Navas, A.; Madrigal-Bustamante, J. A.; Graue-Hernandez, E. O., Current Global Bioethical Dilemmas in Corneal Transplantation. *Cornea* **9000,** *Publish Ahead of Print.*
75. Okumura, N.; Koizumi, N.; Ueno, M.; Sakamoto, Y.; Takahashi, H.; Hirata, K.; Torii, R.; Hamuro, J.; Kinoshita, S., Enhancement of corneal endothelium wound healing by Rho-associated kinase (ROCK) inhibitor eye drops. *British Journal of Ophthalmology* **2011,** *95* (7), 1006.
76. Pipparelli, A.; Arsenijevic, Y.; Thuret, G.; Gain, P.; Nicolas, M.; Majo, F., ROCK Inhibitor Enhances Adhesion and Wound Healing of Human Corneal Endothelial Cells. *PLOS ONE* **2013,** *8* (4), e62095.
77. Okumura, N.; Koizumi, N.; Kay, E. P.; Ueno, M.; Sakamoto, Y.; Nakamura, S.; Hamuro, J.; Kinoshita, S., The ROCK Inhibitor Eye Drop Accelerates Corneal Endothelium Wound Healing. *Investigative Ophthalmology & Visual Science* **2013,** *54* (4), 2493-2502.
78. Okumura, N.; Nakano, S.; Kay, E. P.; Numata, R.; Ota, A.; Sowa, Y.; Sakai, T.; Ueno, M.; Kinoshita, S.; Koizumi, N., Involvement of Cyclin D and p27 in Cell Proliferation Mediated by ROCK Inhibitors Y-27632 and Y-39983 During Corneal Endothelium Wound Healing. *Investigative Ophthalmology & Visual Science* **2014,** *55* (1), 318-329.
79. Kim, E. C.; Toyono, T.; Berlinicke, C. A.; Zack, D. J.; Jurkunas, U.; Usui, T.; Jun, A. S., Screening and Characterization of Drugs That Protect Corneal Endothelial Cells Against Unfolded

Protein Response and Oxidative Stress. *Investigative Ophthalmology & Visual Science* **2017,** *58* (2), 892-900.
80. Shima, N.; Kimoto, M.; Yamaguchi, M.; Yamagami, S., Increased Proliferation and Replicative Lifespan of Isolated Human Corneal Endothelial Cells with l-Ascorbic acid 2-phosphate. *Investigative Ophthalmology & Visual Science* **2011,** *52* (12), 8711-8717.
81. Soh, Y. Q.; Peh, G.; George, B. L.; Seah, X. Y.; Primalani, N. K.; Adnan, K.; Mehta, J. S., Predicative Factors for Corneal Endothelial Cell Migration. *Investigative Ophthalmology & Visual Science* **2016,** *57* (2), 338-348.
82. Bhogal, M.; Lwin, C. N.; Seah, X.-Y.; Peh, G.; Mehta, J. S., Allogeneic Descemet's Membrane Transplantation Enhances Corneal Endothelial Monolayer Formation and Restores Functional Integrity Following Descemet's Stripping. *Investigative Ophthalmology & Visual Science* **2017,** *58* (10), 4249-4260.
83. Soh, Y. Q.; Peh, G. S. L.; Mehta, J. S., Translational issues for human corneal endothelial tissue engineering. *Journal of Tissue Engineering and Regenerative Medicine* **2017,** *11* (9), 2425-2442.
84. Bostan, C.; Thériault, M.; Forget, K. J.; Doyon, C.; Cameron, J. D.; Proulx, S.; Brunette, I., In Vivo Functionality of a Corneal Endothelium Transplanted by Cell-Injection Therapy in a Feline Model. *Investigative Ophthalmology & Visual Science* **2016,** *57* (4), 1620-1634.
85. Okumura, N.; Kinoshita, S.; Koizumi, N., Cell-Based Approach for Treatment of Corneal Endothelial Dysfunction. *Cornea* **2014,** *33*.
86. Lanzalaco, S.; Armelin, E., Poly(N-isopropylacrylamide) and Copolymers: A Review on Recent Progresses in Biomedical Applications. *Gels* **2017,** *3* (4).
87. Nitschke, M.; Gramm, S.; Götze, T.; Valtink, M.; Drichel, J.; Voit, B.; Engelmann, K.; Werner, C., Thermo-responsive poly(NiPAAm-co-DEGMA) substrates for gentle harvest of human corneal endothelial cell sheets. *Journal of Biomedical Materials Research Part A* **2007,** *80A* (4), 1003-1010.
88. Hsiue, G.-H.; Lai, J.-Y.; Chen, K.-H.; Hsu, W.-M., A Novel Strategy for Corneal Endothelial Reconstruction with a Bioengineered Cell Sheet. *Transplantation* **2006,** *81* (3).
89. Rizwan, M.; Peh, G. S. L.; Ang, H.-P.; Lwin, N. C.; Adnan, K.; Mehta, J. S.; Tan, W. S.; Yim, E. K. F., Sequentially-crosslinked bioactive hydrogels as nano-patterned substrates with customizable stiffness and degradation for corneal tissue engineering applications. *Biomaterials* **2017,** *120*, 139-154.
90. Kim, D. K.; Sim, B. R.; Kim, J. I.; Khang, G., Functionalized silk fibroin film scaffold using β-Carotene for cornea endothelial cell regeneration. *Colloids and Surfaces B: Biointerfaces* **2018,** *164*, 340-346.
91. Kennedy, S.; Lace, R.; Carserides, C.; Gallagher, A. G.; Wellings, D. A.; Williams, R. L.; Levis, H. J., Poly-ε-lysine based hydrogels as synthetic substrates for the expansion of corneal endothelial cells for transplantation. *Journal of Materials Science: Materials in Medicine* **2019,** *30* (9), 102.
92. Wang, T.-J.; Wang, I. J.; Hu, F.-R.; Young, T.-H., Applications of Biomaterials in Corneal Endothelial Tissue Engineering. *Cornea* **2016,** *35*.
93. Wojtkowiak-Szlachcic, A.; Taylor, K.; Stepniak-Konieczna, E.; Sznajder, L. J.; Mykowska, A.; Sroka, J.; Thornton, C. A.; Sobczak, K., Short antisense-locked nucleic acids (all-LNAs) correct alternative splicing abnormalities in myotonic dystrophy. *Nucleic Acids Research* **2015,** *43* (6), 3318-3331.
94. Gao, Z.; Cooper, T. A., Antisense oligonucleotides: rising stars in eliminating RNA toxicity in myotonic dystrophy. *Human gene therapy.* **2013,** *24* (5), 499-507.
95. Nguyen, A. T.; Sathe, S. R.; Yim, E. K. F., From nano to micro: topographical scale and its impact on cell adhesion, morphology and contact guidance. *Journal of Physics: Condensed Matter* **2016,** *28* (18), 183001.
96. Engler, A. J.; Sen, S.; Sweeney, H. L.; Discher, D. E., Matrix Elasticity Directs Stem Cell Lineage Specification. *Cell* **2006,** *126* (4), 677-689.

97. Wells, R. G., The role of matrix stiffness in regulating cell behavior. *Hepatology* **2008,** *47* (4), 1394-1400.
98. Abrams, G. A.; Schaus, S. S.; Goodman, S. L.; Nealey, P. F.; Murphy, C. J., Nanoscale Topography of the Corneal Epithelial Basement Membrane and Descemet's Membrane of the Human. *Cornea* **2000,** *19* (1).
99. Koo, S.; Muhammad, R.; Peh, G. S. L.; Mehta, J. S.; Yim, E. K. F., Micro- and nanotopography with extracellular matrix coating modulate human corneal endothelial cell behavior. *Acta Biomaterialia* **2014,** *10* (5), 1975-1984.
100. Muhammad, R.; Peh, G. S. L.; Adnan, K.; Law, J. B. K.; Mehta, J. S.; Yim, E. K. F., Micro- and nano-topography to enhance proliferation and sustain functional markers of donor-derived primary human corneal endothelial cells. *Acta Biomaterialia* **2015,** *19*, 138-148.
101. Teo, B. K. K.; Goh, K. J.; Ng, Z. J.; Koo, S.; Yim, E. K. F., Functional reconstruction of corneal endothelium using nanotopography for tissue-engineering applications. *Acta Biomaterialia* **2012,** *8* (8), 2941-2952.
102. Discher, D. E.; Janmey, P.; Wang, Y.-l., Tissue Cells Feel and Respond to the Stiffness of Their Substrate. *Science* **2005,** *310* (5751), 1139.
103. Xia, D.; Zhang, S.; Nielsen, E.; Ivarsen, A. R.; Liang, C.; Li, Q.; Thomsen, K.; Hjortdal, J. Ø.; Dong, M., The Ultrastructures and Mechanical Properties of the Descement's Membrane in Fuchs Endothelial Corneal Dystrophy. *Scientific Reports* **2016,** *6*, 23096.
104. Palchesko, R. N.; Lathrop, K. L.; Funderburgh, J. L.; Feinberg, A. W., In Vitro Expansion of Corneal Endothelial Cells on Biomimetic Substrates. *Scientific Reports* **2015,** *5* (1), 7955.
105. Borderie, V. M.; Baudrimont, M.; Vallée, A.; Ereau, T. L.; Gray, F. o.; Laroche, L., Corneal Endothelial Cell Apoptosis in Patients with Fuchs' Dystrophy. *Investigative Ophthalmology & Visual Science* **2000,** *41* (9), 2501-2505.
106. Li, Q. J.; Ashraf, M. F.; Shen, D.; Green, W. R.; Stark, W. J.; Chan, C.-C.; O'Brien, T. P., The Role of Apoptosis in the Pathogenesis of Fuchs Endothelial Dystrophy of the Cornea. *Archives of Ophthalmology* **2001,** *119* (11), 1597-1604.
107. Szentmáry, N.; Szende, B.; Süveges, I., Epithelial Cell, Keratocyte, and Endothelial Cell Apoptosis in Fuchs' Dystrophy and in Pseudophakic Bullous Keratopathy. *European Journal of Ophthalmology* **2005,** *15* (1), 17-22.
108. Elmore, S., Apoptosis: A Review of Programmed Cell Death. *Toxicologic Pathology* **2007,** *35* (4), 495-516.
109. Charras, G. T., A short history of blebbing. *Journal of Microscopy* **2008,** *231* (3), 466-478.
110. Tinevez, J.-Y.; Schulze, U.; Salbreux, G.; Roensch, J.; Joanny, J.-F.; Paluch, E., Role of cortical tension in bleb growth. *Proceedings of the National Academy of Sciences* **2009,** *106* (44), 18581.
111. Zhang, Y.; Chen, X.; Gueydan, C.; Han, J., Plasma membrane changes during programmed cell deaths. *Cell Research* **2018,** *28* (1), 9-21.
112. Rysavy, N. M.; Shimoda, L. M. N.; Dixon, A. M.; Speck, M.; Stokes, A. J.; Turner, H.; Umemoto, E. Y., Beyond apoptosis: the mechanism and function of phosphatidylserine asymmetry in the membrane of activating mast cells. *Bioarchitecture.* **2014,** *4* (4-5), 127-137.
113. Dai, J.; Sheetz, M. P., Membrane Tether Formation from Blebbing Cells. *Biophysical Journal* **1999,** *77* (6), 3363-3370.
114. Gauthier, N. C.; Masters, T. A.; Sheetz, M. P., Mechanical feedback between membrane tension and dynamics. *Trends in Cell Biology* **2012,** *22* (10), 527-535.
115. Ndozangue-Touriguine, O.; Hamelin, J.; Bréard, J., Cytoskeleton and apoptosis. *Biochemical Pharmacology* **2008,** *76* (1), 11-18.
116. Sebbagh, M.; Renvoizé, C.; Hamelin, J.; Riché, N.; Bertoglio, J.; Bréard, J., Caspase-3-mediated cleavage of ROCK I induces MLC phosphorylation and apoptotic membrane blebbing. *Nature Cell Biology* **2001,** *3* (4), 346-352.
117. Chang, J.; Xie, M.; Shah, V. R.; Schneider, M. D.; Entman, M. L.; Wei, L.; Schwartz, R. J., Activation of Rho-associated coiled-coil protein kinase 1 (ROCK-1) by caspase-3 cleavage plays an

essential role in cardiac myocyte apoptosis. *Proceedings of the National Academy of Sciences* **2006,** *103* (39), 14495.
118. Shi, J.; Wu, X.; Surma, M.; Vemula, S.; Zhang, L.; Yang, Y.; Kapur, R.; Wei, L., Distinct roles for ROCK1 and ROCK2 in the regulation of cell detachment. *Cell Death & Disease* **2013,** *4* (2), e483-e483.
119. Croft, D. R.; Coleman, M. L.; Li, S.; Robertson, D.; Sullivan, T.; Stewart, C. L.; Olson, M. F., Actin-myosin–based contraction is responsible for apoptotic nuclear disintegration. *Journal of Cell Biology* **2005,** *168* (2), 245-255.
120. Orlando, K. A.; Stone, N. L.; Pittman, R. N., Rho kinase regulates fragmentation and phagocytosis of apoptotic cells. *Experimental Cell Research* **2006,** *312* (1), 5-15.
121. Song, Y.; Hoang, B. Q.; Chang, D. D., ROCK-II-Induced Membrane Blebbing and Chromatin Condensation Require Actin Cytoskeleton. *Experimental Cell Research* **2002,** *278* (1), 45-52.
122. Coleman, M. L.; Sahai, E. A.; Yeo, M.; Bosch, M.; Dewar, A.; Olson, M. F., Membrane blebbing during apoptosis results from caspase-mediated activation of ROCK I. *Nature Cell Biology* **2001,** *3* (4), 339-345.
123. Hébert, M.; Potin, S.; Sebbagh, M.; Bertoglio, J.; Bréard, J.; Hamelin, J., Rho-ROCK-Dependent Ezrin-Radixin-Moesin Phosphorylation Regulates Fas-Mediated Apoptosis in Jurkat Cells. *The Journal of Immunology* **2008,** *181* (9), 5963.
124. Shi, J.; Wei, L., Rho kinase in the regulation of cell death and survival. *Archivum Immunologiae et Therapiae Experimentalis* **2007,** *55* (2), 61.
125. Valtink, M.; Gruschwitz, R.; Funk, R. H. W.; Engelmann, K., Two Clonal Cell Lines of Immortalized Human Corneal Endothelial Cells Show either Differentiated or Precursor Cell Characteristics. *Cells Tissues Organs* **2008,** *187* (4), 286-294.
126. Frausto, R. F.; Le, D. J.; Aldave, A. J., Transcriptomic Analysis of Cultured Corneal Endothelial Cells as a Validation for Their Use in Cell Replacement Therapy. *Cell Transplantation* **2016,** *25* (6), 1159-1176.
127. Okumura, N.; Koizumi, N.; Ueno, M.; Sakamoto, Y.; Takahashi, H.; Tsuchiya, H.; Hamuro, J.; Kinoshita, S., ROCK Inhibitor Converts Corneal Endothelial Cells into a Phenotype Capable of Regenerating In Vivo Endothelial Tissue. *The American Journal of Pathology* **2012,** *181* (1), 268-277.
128. Peh, G. S. L.; Ong, H. S.; Adnan, K.; Ang, H.-P.; Lwin, C. N.; Seah, X.-Y.; Lin, S.-J.; Mehta, J. S., Functional Evaluation of Two Corneal Endothelial Cell-Based Therapies: Tissue-Engineered Construct and Cell Injection. *Scientific Reports* **2019,** *9* (1), 6087.
129. Desouza, M.; Gunning, P. W.; Stehn, J. R., The actin cytoskeleton as a sensor and mediator of apoptosis. *BioArchitecture* **2012,** *2* (3), 75-87.
130. Jain, D.; Mattiassi, S.; Goh, E.; Yim, E., Extracellular matrix and biomimetic engineering microenvironment for neuronal differentiation. **2020,** *15* (4), 573-585.
131. Lovatt, M.; Adnan, K.; Kocaba, V.; Dirisamer, M.; Peh, G. S. L.; Mehta, J. S., Peroxiredoxin-1 regulates lipid peroxidation in corneal endothelial cells. *Redox Biology* **2020,** *30*, 101417.
132. Ganesan, M.; Dagur, R. S.; Makarov, E.; Poluektova, L. I.; Kidambi, S.; Osna, N. A., Matrix stiffness regulate apoptotic cell death in HIV-HCV co-infected hepatocytes: Importance for liver fibrosis progression. *Biochemical and Biophysical Research Communications* **2018,** *500* (3), 717-722.
133. Gouveia, R. M.; Lepert, G.; Gupta, S.; Mohan, R. R.; Paterson, C.; Connon, C. J., Assessment of corneal substrate biomechanics and its effect on epithelial stem cell maintenance and differentiation. *Nature Communications* **2019,** *10* (1), 1496.
134. Masterton, S.; Ahearne, M., Mechanobiology of the corneal epithelium. *Experimental eye research* **2018,** *177*, 122-129.
135. Amit, C.; Padmanabhan, P.; Elchuri, S. V.; Narayanan, J., Probing the effect of matrix stiffness in endocytic signalling pathway of corneal epithelium. *Biochemical and Biophysical Research Communications* **2020**.
136. Frantz, C.; Stewart, K. M.; Weaver, V. M., The extracellular matrix at a glance. *Journal of Cell Science* **2010,** *123* (24), 4195.

137. Chu, G.; Yuan, Z.; Zhu, C.; Zhou, P.; Wang, H.; Zhang, W.; Cai, Y.; Zhu, X.; Yang, H.; Li, B., Substrate stiffness- and topography-dependent differentiation of annulus fibrosus-derived stem cells is regulated by Yes-associated protein. *Acta Biomaterialia* **2019,** *92*, 254-264.
138. Wu, Y.; Yang, Z.; Law, J. B. K.; He, A. Y.; Abbas, A. A.; Denslin, V.; Kamarul, T.; Hui, J. H. P.; Lee, E. H., The Combined Effect of Substrate Stiffness and Surface Topography on Chondrogenic Differentiation of Mesenchymal Stem Cells. *Tissue Engineering Part A* **2016,** *23* (1-2), 43-54.
139. Yue, K.; Trujillo-de Santiago, G.; Alvarez, M. M.; Tamayol, A.; Annabi, N.; Khademhosseini, A., Synthesis, properties, and biomedical applications of gelatin methacryloyl (GelMA) hydrogels. *Biomaterials* **2015,** *73*, 254-271.
140. Yam, H. G.; Seah, X.; Yusoff, Z. N.; Setiawan, M.; Wahlig, S.; Htoon, M. H.; Peh, S. L. G.; Kocaba, V.; Mehta, S. J., Characterization of Human Transition Zone Reveals a Putative Progenitor-Enriched Niche of Corneal Endothelium. *Cells* **2019,** *8* (10).
141. MicroTester G2:Micro-scale Tension-Compression Test System User Manual 4.0. *Cellscale biomaterials testing* **2018**.
142. Patel, S.; Tutchenko, L., The refractive index of the human cornea: A review. *Contact Lens and Anterior Eye* **2019,** *42* (5), 575-580.
143. Compression testing of soft materials *Cellscale biomaterials testing* **2016**.
144. Last, J. A.; Liliensiek, S. J.; Nealey, P. F.; Murphy, C. J., Determining the mechanical properties of human corneal basement membranes with atomic force microscopy. *Journal of Structural Biology* **2009,** *167* (1), 19-24.
145. Guimarães, C. F.; Gasperini, L.; Marques, A. P.; Reis, R. L., The stiffness of living tissues and its implications for tissue engineering. *Nature Reviews Materials* **2020,** *5* (5), 351-370.
146. Gilbert, P. M.; Havenstrite, K. L.; Magnusson, K. E. G.; Sacco, A.; Leonardi, N. A.; Kraft, P.; Nguyen, N. K.; Thrun, S.; Lutolf, M. P.; Blau, H. M., Substrate Elasticity Regulates Skeletal Muscle Stem Cell Self-Renewal in Culture. *Science* **2010,** *329* (5995), 1078.
147. Chaudhuri, O.; Gu, L.; Klumpers, D.; Darnell, M.; Bencherif, S. A.; Weaver, J. C.; Huebsch, N.; Lee, H.-p.; Lippens, E.; Duda, G. N.; Mooney, D. J., Hydrogels with tunable stress relaxation regulate stem cell fate and activity. *Nature Materials* **2016,** *15* (3), 326-334.
148. Hlady, V.; Buijs, J., Protein adsorption on solid surfaces. *Current Opinion in Biotechnology* **1996,** *7* (1), 72-77.
149. Ayee, M. A. A.; LeMaster, E.; Teng, T.; Lee, J.; Levitan, I., Hypotonic Challenge of Endothelial Cells Increases Membrane Stiffness with No Effect on Tether Force. *Biophysical Journal* **2018,** *114* (4), 929-938.
150. Colom, A.; Derivery, E.; Soleimanpour, S.; Tomba, C.; Molin, M. D.; Sakai, N.; González-Gaitán, M.; Matile, S.; Roux, A., A fluorescent membrane tension probe. *Nature Chemistry* **2018,** *10* (11), 1118-1125.
151. Julian, L.; Olson, M. F., Rho-associated coiled-coil containing kinases (ROCK). *Small GTPases* **2014,** *5* (2), e29846.